REPORT DOCUMENTATION PAGE

Form Approved OMB NO. 0704-0188

1. REPORT DATE (DD-MM-YYYY)	2. REPORT TYPE	3. DATES COVERED (From - To)
24-10-2012	Final Report	1-Jul-2006 - 30-Jun-2012

4. TITLE AND SUBTITLE
Superatoms as Building Blocks of New Materials

5a. CONTRACT NUMBER
W911NF-06-1-0280

5b. GRANT NUMBER

5c. PROGRAM ELEMENT NUMBER
611103

6. AUTHORS
A. Sen S. Khanna, Jr., A. W. Castleman Jr.

5d. PROJECT NUMBER

5e. TASK NUMBER

5f. WORK UNIT NUMBER

7. PERFORMING ORGANIZATION NAMES AND ADDRESSES
Pennsylvania State University
Office of Sponsored Programs
The Pennsylvania State University
University Park, PA 16802 -7000

8. PERFORMING ORGANIZATION REPORT NUMBER

9. SPONSORING/MONITORING AGENCY NAME(S) AND ADDRESS(ES)
U.S. Army Research Office
P.O. Box 12211
Research Triangle Park, NC 27709-2211

10. SPONSOR/MONITOR'S ACRONYM(S)
ARO

11. SPONSOR/MONITOR'S REPORT NUMBER(S)
50344-MS-MUR.82

12. DISTRIBUTION AVAILIBILITY STATEMENT
Approved for Public Release; Distribution Unlimited

13. SUPPLEMENTARY NOTES
The views, opinions and/or findings contained in this report are those of the author(s) and should not contrued as an official Department of the Army position, policy or decision, unless so designated by other documentation.

14. ABSTRACT
During the last couple of decades or so, the subject of nanoscale science began expanding into a unique field of science that offered the prospect of tailoring the design of materials having chosen properties. Two potentially promising approaches were conceived, one involving a bottom up approach while the other a top down method. In both cases, approaching the desirable nanoscale size regime where the properties of matter began to display nonlinear scalable behavior in which each atom counts, the connection to the area of cluster science began to be

15. SUBJECT TERMS
superatoms, building blocks materials, nanoscale, alkali metals

16. SECURITY CLASSIFICATION OF:			17. LIMITATION OF ABSTRACT	15. NUMBER OF PAGES	19a. NAME OF RESPONSIBLE PERSON
a. REPORT	b. ABSTRACT	c. THIS PAGE			Albert Castleman
UU	UU	UU	UU		19b. TELEPHONE NUMBER 814-865-7242

Report Title

Superatoms as Building Blocks of New Materials

ABSTRACT

During the last couple of decades or so, the subject of nanoscale science began expanding into a unique field of science that offered the prospect of tailoring the design of materials having chosen properties. Two potentially promising approaches were conceived, one involving a bottom up approach while the other a top down method. In both cases, approaching the desirable nanoscale size regime where the properties of matter began to display nonlinear scalable behavior in which each atom counts, the connection to the area of cluster science began to be realized. Four well established academic groups (Castleman—PSU; Khanna---VCU; Sen---PSU; Weiss---PSU) successfully responded to a call for a MURI proposal with the eventual objective of expanding the concept of employing clusters and related superatoms for the use of building blocks for designing matter of nanoscale dimensions with tailored properties. The four groups, which had a history of closely interacting, fashioned a comprehensive research program to lay out the fundamentals for exploring the bottom up approach to design and produce new building blocks for several classes of systems including metals and alloys, metal compounds, metalloids, zintl ions and covalently bound species. Beyond the above, a major objective was to lay the foundation for producing materials with selected band gaps.

Enter List of papers submitted or published that acknowledge ARO support from the start of the project to the date of this printing. List the papers, including journal references, in the following categories:

(a) Papers published in peer-reviewed journals (N/A for none)

Received	Paper	
01/16/2013	86.00	K. Don Dasitha Gunaratne, Cuneyt Berkdemir, Christopher L. Harmon, A. W. Castleman. Investigating the Relative Stabilities and Electronic Properties of Small Zinc Oxide Clusters, The Journal of Physical Chemistry A, (12 2012): 0. doi: 10.1021/jp3029374
01/27/2011	51.00	U. Gupta, J. Reveles, J. Melko, S. Khanna, A. Castleman Jr.. Electron delocalization in a non-cyclic all-metal III-V cluster, Chemical Physics Letters, (09 2009): . doi:
01/27/2011	50.00	D. Hydutsky, N. Bianco, A. Castleman Jr. Photodissociation of SO2 at 200 nm: Evidence of an anisotrophy effect, , (02 2011): . doi:
02/19/2009	24.00	M. Sobhy, J. Reveles, U. Gupta, S. Khanna, A. Castleman, Jr.. Photoelectron Imaging and Theoretical Investigation of Bimetallic Bi1-2Ga0-2- and Lead Pb1-4- Cluster Anions, Journal of Chemical Physics, (2009): . doi:
02/19/2009	25.00	A. Castleman, Jr., S. Khanna. Clusters, Superatoms, and Building Blocks of New Materials, Journal of Physical Chemistry, (2009): . doi:
02/19/2009	26.00	S. Claridge, A. Castleman, Jr., S. Khanna, C. Murray, A. Sen, P. Weiss. Cluster-Assembled Materials, , ( ): . doi:
05/11/2011	61.00	A. W. Castleman, Jr.. From Elements to Clusters: The Periodic Table Revisited, Journal of Physical Chemistry Letters, (04 2011): . doi:
07/01/2011	62.00	K. D. D. Gunaratne, A. Hazra, and A. W. Castleman, Jr.. Photoelectron Imaging Spectroscopy and Theoretical Investigation of ZrSi, Journal of Chemical Physics, (05 2011): . doi:
07/07/2012	63.00	A. W. Castleman. Cluster Structure and Reactions: Gaining Insights into Catalytic Processes, Catalysis Letters, (08 2011): 1243. doi: 10.1007/s10562-011-0670-7
07/07/2012	70.00	K. Franzreb, J. N. Harvey, S. G. Sayres, M. W. Ross, D. E. Blumling, V. Brites, A. W. Castleman, M. Hochlaf. Oxygen-containing gas-phase diatomic trications and tetracations: ReOz+, NbOz+ and HfOz+ (z = 3, 4), Physical Chemistry Chemical Physics, (07 2011): 0. doi: 10.1039/c1cp21566c
07/07/2012	69.00	Joshua J. Melko, Ute Werner, Roland Mitric?, Vlasta Bonac?ic?-Koutecky?, A. W. Castleman. Electronic Structure Similarities in Pb, The Journal of Physical Chemistry A, (08 2011): 10276. doi: 10.1021/jp207474h
07/22/2010	36.00	Joshua J. Melko, S. Vincent Ong, Ujjwal Gupta, J. Ulises Reveles, Jonathan D'Emidio, Shiv N. Khanna, A. W. Castleman Jr.. Resilient Aromaticity in Lead-Indium Clusters, Chemical Physics Letters, (07 2010): . doi:
07/22/2010	37.00	Meichun Qian, Arthur C. Reber, Angel Ugrinov, Nirmalya K. Chaki, Sukhendu Mandal, Hector M. Saavedra, Shiv N. Khanna, , Ayusman Sen, , Paul S. Weiss. Cluster-Assembled Materials: Toward Nanomaterials with Precise Control over Properties, ACS Nano, (07 2010): . doi:
07/22/2010	38.00	H´ector M Saavedra, Thomas J Mullen, Pengpeng Zhang, Daniel C Dewey, Shelley A Claridge, Paul S Weiss. Hybrid strategies in nanolithography, Rep Prog Physics, (01 2010): . doi:

09/28/2010	43.00	Nirmalya Chaki, Sukhendu Mandal, Arthur Reber, Meichun Qian, Hector Saavedra, Paul Weiss, Shiv Khanna, Ayusman Sen. Controlling Band Gap Energies in Cluster-Assembled Ionic Solids through Internal Electric Fields, ACS Nano, (09 2010): . doi:
10/23/2012	72.00	Ayusman Sen, Sukhendu Mandal, Arthur C. Reber, Meichun Qian, Ran Liu, Hector M. Saavedra, Saikat Sen, Paul S. Weiss, Shiv N. Khanna. Synthesis, structure and band gap energy of covalently linked cluster-assembled materials, Dalton Transactions, (08 2012): 0. doi: 10.1039/c2dt31286g
10/23/2012	77.00	Sukhendu Mandal, Ran Liu, Arthur C. Reber, Meichun Qian, Héctor M. Saavedra, Xianglin Ke, Peter Schiffer, Saikat Sen, Paul S. Weiss, Shiv N. Khanna, Ayusman Sen. The Zintl ion [As7]2?: an example of an electron-deficient Asx radical anion, Chemical Communications, (01 2011): 0. doi: 10.1039/c0cc03219k
10/23/2012	76.00	Sukhendu Mandal, Arthur C. Reber, Meichun Qian, Ran Liu, Hector M. Saavedra, Saikat Sen, Paul S. Weiss, Shiv N. Khanna, Ayusman Sen. On the stability of an unsupported mercury–mercury bond linking group 15 Zintl clusters, Dalton Transactions, (02 2012): 0. doi: 10.1039/c2dt30083d
10/23/2012	75.00	Arthur C. Reber, Sukhendu Mandal, Meichun Qian, Hector M. Saavedra, Paul S. Weiss, Shiv N. Khanna, Ayusman Sen. Palladium in the Gap: Cluster Assemblies with Band Edges Localized on Linkers, The Journal of Physical Chemistry C, (05 2012): 0. doi: 10.1021/jp301049e
10/24/2012	79.00	Meichun Qian, Arthur C. Reber, Angel Ugrinov, Nirmalya K. Chaki, Sukhendu Mandal, He?ctor M. Saavedra, Shiv N. Khanna, Ayusman Sen, Paul S. Weiss. Cluster-Assembled Materials: Toward Nanomaterials with Precise Control over Properties, ACS Nano, (01 2010): 0. doi: 10.1021/nn9010297
11/01/2010	47.00	K. Don Dasitha Gunaratne, A. W. Castleman Jr.. Photoelectron imaging spectroscopy and theoretical investigation of ZrSi , Journal of Chemical Physics, (11 2010): . doi:
12/11/2012	83.00	I. Iordanov, K. D. D. Gunaratne, C. L. Harmon, J. O. Sofo, A. W. Castleman. Broad photoelectron spectrum and lowered electron affinity due to hydrogen in ZnOH: A joint experimental and theoretical study, The Journal of Chemical Physics, (11 2012): 0. doi: 10.1063/1.4725713
12/11/2012	84.00	Matt W. Ross, A. W. Castleman. Ionization enhancement in silicon clusters and germanium atoms in the presence of zirconium, The Journal of Chemical Physics, (11 2012): 0. doi: 10.1063/1.4766935
TOTAL:	**23**	

Number of Papers published in peer-reviewed journals:

(b) Papers published in non-peer-reviewed journals (N/A for none)

Received		Paper
08/01/2008	5.00	Jr., S.N. Khanna, A.C. Reber, A.W. Castleman. Superatom Compounds, Clusters and Assemblies: Ultra Alkali Motifs and Novel Architectures, Journal of the American Chemical Society, ( ): . doi:
08/01/2008	8.00	Arthur C. Reber, Shiv N. Khanna, A. Welford Castleman, Jr., William H. Woodward, Patrick J. Roach. Spin Accommodation and Reactivity of Aluminum Based Clusters with O2, , ( ): . doi:
10/23/2012	73.00	S. Mandal, M. Qian, A. C. Reber, H. M. Saavedra, P. S. Weiss, S. N. Khanna, A. Sen. [As7M(CO)3]3– M = Cr, Mo, W: Bonding and Electronic Structure of Cluster Assemblies with Metal Carbonyls, J. Phys. Chem. C, (10 2011): 23704. doi:
TOTAL:		**3**

Number of Papers published in non peer-reviewed journals:

(c) Presentations

"Influence of Clustering and Molecular Orbital Shapes on Ionization Enhancement and Coulomb Explosion of Molecular Systems", (A. W. Castleman, Jr.,), CERF 2011, Rostock, Germany, September 12-16, 2011.

"Sonochemical Synthesis of Transition Metal Carbide", (D. M. David Jeba Singh – poster, and A. W. Castleman, Jr..), International Symposium on Clusters and Nanostructures, Richmond, VA, November 7 – 10, 2011.

"Gas-Phase Reactivity of Aluminum and Copper Cluster Anions", (Zhixun Luo – Poster, Jordan Smith, William Woodward and A. W. Castleman, Jr.), International Symposium on Clusters and Nanostructures, Richmond, VA, November 7 – 10, 2011.

"Extreme Ionization of Molecules and Clusters Leading to Coulomb Explosion", (Matt Ross – Poster, Scott Sayres and A. W. Castleman, Jr.), International Symposium on Clusters and Nanostructures, Richmond, VA, November 7 – 10, 2011.

"Carbonyl Bond Cleavage by Complimentary Active Sites", (Jordan Smith – Poster, William Woodward, Arthur Reber, Shiv Khanna and A. W. Castleman, Jr.), International Symposium on Clusters and Nanostructures, Richmond, VA, November 7 – 10, 2011.

"Model Studies in Catalysis Through Cluster Research", (A. W. Castleman, Jr.), Utah MURI review, Salt Lake City, Utah, December 6-7, 2011.

"Structure and Stability of the M8-nNnC12 (M=Ti, Zr; N-Sc, Y and n-1,2,3) Met-Cars as Building Blocks of Cluster-Assembled Materials", (Contributed talk by C. Berkdemir), APS March Meeting, Boston, MA February 27 – Mach 2, 2012.

"Cooperative Effects in the Oxidation of CO by Palladium Oxide Cations", (Contributed Talk by A. C. Reber), APS March Meeting, Boston, MA February 27 – Mach 2, 2012.

"Breaking Carbonyl Bonds in Formaldehyde via Complementary Active Sites", (Contributed Talk by S. N. Khanna), APS March Meeting, Boston, MA February 27 – Mach 2, 2012.

"Photoelectron Angular Distributions of Transition Metal Dioxide Anions – A joint Experimental and Theoretical Study", (Contributed talk by: I. Iordanov) APS March Meeting, Boston, MA February 27 – Mach 2, 2012.

"The Periodic Table Revistied", Evan Pugh Meeting, Penn State University, April 26, 2012.

Number of Presentations: 10.00

Non Peer-Reviewed Conference Proceeding publications (other than abstracts):

Received	Paper

TOTAL:

Number of Non Peer-Reviewed Conference Proceeding publications (other than abstracts):

Peer-Reviewed Conference Proceeding publications (other than abstracts):

Received	Paper

TOTAL:

Number of Peer-Reviewed Conference Proceeding publications (other than abstracts):

(d) Manuscripts

Received	Paper	
01/08/2010	29.00	U. Gupta, J. Reveles, J. Melko, S. Khanna, A. Castleman. Origins of Stability in Mixed Bismuth-Indium Clusters, (08 2011)
01/27/2011	52.00	W. Woodward, M. Blake, P. Roach, J. Smith, A. Kurland, P. Han, P. Weiss, A. Castleman Jr.. Versatile Portable Vacuum Suitcase with Stable Sample Transfer Capabilities, (02 2011)
02/03/2009	22.00	R. Robles, S.N. Khanna. Stable T2Sin (T=Fe,Co,Ni,1<n<8) Cluster Motifs, ( )
02/03/2009	23.00	J. U. Reveles, P.A. Clayborne, A.C. Rever, S.N. Khanna, K. Pradhan, P. Sen, M.R. Pederson. Designer Magnetic Superatoms, ( )
02/08/2010	30.00	S. V. Ong, R. Robles, S. N. Khanna. Evolution of Graphene Mediated Magnetic Coupling Between Fe-Chains, Physical Review B (02 2010)
02/08/2010	31.00	J. J. Melko, P. A. Clayborne, C. E. Jones, Jr., J. U. Reveles, U. Gupta, S. N. Khanna, A. W. Castleman, Jr.. Combined Experimental and Theoretical Study of AlnX (n) 1-6; X) As, Sb) Clusters: Evidence of Aromaticity and the Jellium Model, Journal of Physical Chemistry A (01 2010)
02/08/2010	32.00	J. Ulises Reveles, Prasenjit Sen, Kalpataru Pradhan, Debesh R. Roya, Shiv N. Khanna. Effect of Electronic and Geometric Shell Closures on the Stability of Neutral and Anionic TiNan (n=1-13) clusters, Chemical Science (02 2010)
02/08/2010	33.00	H. He, R. Pandey, J. Ulises Reveles, S. N. Khanna, S. P. Karna. Highly efficient (Cs8V) superatom-based spin-polarizer, Applied Physics Letters (11 2009)
02/23/2009	27.00	R. Robles, S. Khanna. Appearance of Magnetism in Supported Silicon Endohedral Cages, ( )
02/23/2011	55.00	Ujjwal Gupta, Arthur C. Reber, Joshua J. Melko, Shiv N. Khanna and A.W. Castleman, Jr.. Stability and Electronic Properties of Isoelectronic Heteroatomic Analogs of Sn52-, Chemical Physics Letters (02 2011)
02/23/2011	54.00	A. C. Reber, S. N. Khanna and A. W. Castleman, Jr.. Superatoms: From Motifs to Materials, Elsevier (12 2010)
02/23/2011	57.00	A. W. Castleman, Jr.. From Elements to Clusters: The Periodic Table Revisited, Journal of Physical Chemistry Letters (02 2011)
02/23/2011	56.00	W. Hunter Woodward, Meaghan M. Blake, Patrick J. Roach, Jordan C. Smith, Adam R. Kurland, Patrick Han, Paul S. Weiss, A. W. Castleman, Jr.. Versatile Portable Vacuum Suitcase with Stable Sample Transfer Capabilities, Review of Scientific Instruments (02 2011)
02/25/2010	35.00	Samuel J. Peppernick, K. D. Dasitha Gunaratne, A. W. Castleman, Jr.. The Relative Abundances of Silicon Hydride Clusters, SinHx? (n = 8 – 12 and 0 ? x ? 25), Investigated with High Resolution Time-of-Flight Mass Spectrometry , International Journal of Mass Spectrometry (12 2009)
03/22/2011	58.00	Joshua J. Melko, Ute Werner, Roland Mitri?, Vlasta Bona?i?-Koutecký, and A. W. Castleman, Jr.. Electronic Structure Similarities in PbxSby- and SnxBiy- Clusters, Journal of Chemical Physics (03 2011)

03/24/2009	28.00	H. M. Saavedra, C. M. Thompson, J. Nathan Hohman, V.H. Crespi, P.S. Weiss. Reversible Lability by in-situ Reaction of Self-Assembled Monolayers, ( )
03/30/2011	59.00	Ujjwal Gupta, Arthur C. Reber, Joshua J. Melko, Shiv N. Khanna, A.W. Castleman Jr.. Stability and electronic properties of isoelectronic heteroatomic analogs of Sn2□, Chemical Physics Letters (02 2011)
04/08/2011	60.00	W. Hunter Woodward, Meaghan M. Blake, Zhixun Luo, Paul S. Weiss, A. W. Castleman, Jr.. Soft-Landing Deposition of Al17 - on a Hydroxyl-Terminated Self-Assembled Monolayer, Journal of Physical Chemistry C (03 2011)
07/07/2012	66.00	Z. Luo, W. H. Woodward, A. W. Castleman, Jr.. Distinguishable Behavior of Multiple and INdividual Rhodamine-6G on Spherical Ag Nanoparticles Examined via Time Dependence of the SERS Spectra, Journal of Raman Spectroscopy (01 2012)
07/07/2012	71.00	K. Don Dasitha Gunaratne, Christopher L. Harmon, A. W. Castleman, Jr.. Formation, Stability and Evolution of Small ZnO-based Clusters in the Gas Phase, Journal of Physical Chemistry (03 2012)
07/22/2010	39.00	Peneé A. Clayborne, Ujjwal Gupta, Arthur C. Reber, Joshua J. Melko, Shiv N. Khanna, A.W. Castleman, Jr.. The Applicability of Three Dimensional Aromaticity in BiSnn- Zintl Analogues, Journal of Chemical Physics (07 2010)
07/22/2010	40.00	M. A. Sobhy, K. Casalenuovo, J. Ulises Reveles, Ujjwal Gupta, Shiv N. Khanna, A. W. Castleman, Jr.. Photoelectron imaging and density-functional investigation of Bismuth and Lead anions solvated in ammonia clusters, Journal of Physical Chemistry A (07 2010)
08/01/2008	7.00	Angel Ugrinov, Ayusman Sen. [Te2As2]2: A Planar Non-Organic Structure with 4n ~-Electrons, ( )
09/23/2010	34.00	U. Gupta, J. Ulises Reveles, J. Melko, S. N. Khanna and A. W. Castleman, Jr.. Origins of Stability in Mixed Bismuth-Indium Clusters, J. Phys. Chem. (03 2010)
09/23/2010	41.00	W. Hunter Woodward, Meaghan M. Blake, Zhixun Luo, Paul S. Weiss, A. W. Castleman, Jr.. Soft-Landing Deposition of Al17- on a Hydroxyl-Terminated Self-Assembled Monolayer, Journal American Chemical Society (09 2010)
09/24/2010	42.00	Joshua J. Melko, S. Vincent Ong, Ujjwal Gupta, J. Ulises Reveles, Jonathan D'Emidio, Shiv N. Khanna, and A. W. Castleman, Jr.. An Anion Photoelectron Spectroscopy and First-Principles Study of PbxIny Clusters, Journal of Physical Chemistry (09 2010)
10/18/2010	44.00	Peneé A. Clayborne, Ujjwal Gupta, Arthur C. Reber, Joshua J. Melko, Shiv N. Khanna, and A. W. Castleman, Jr.. The Applicability of Three-Dimensional Aromaticity in BiSnn- Zintl Analogues, Journal of Chemical Physics (10 2010)
10/24/2012	78.00	Nirmalya K. Chaki, Sukhendu Mandal, Arthur C. Reber, Meichun Qian, Hector M. Saavedra, Paul S. Weiss, Shiv N. Khanna, Ayusman Sen. Controlling Band Gap Energies inCluster-Assembled Ionic Solids throughInternal Electric Fields, ACS Nano (09 2010)
10/24/2012	81.00	Matt Ross, A. W. Castleman, Jr.. Ionization Enhancement in Small Silicon and Germanium Clusters in the Presence of Zirconium, Journal of Chemical Physics (09 2012)
10/24/2012	80.00	K. Don Dasitha Gunaratne, Cuneyt Berkdemir, Christopher L. Harmon, A. W. Castleman, Jr.. Experimental and Theoretical Investigation of Small ZnO-based Clusters, Journal of Physical Chemistry (07 2012)

11/01/2010	45.00	Mohamed A. Sobhy, K. Casalenuovo, J. Ulises Reveles, Ujjwal Gupta, Shiv N. Khanna, and A. W. Castleman, Jr.. Photoelectron Imaging and Density-Functional Investigation of Bismuth and Lead Anions Solvated in Ammonia Clusters, J. Phys. Chem. (08 2010)
11/01/2010	46.00	Nirmalya K. Chaki, Sukhendu Mandal, Arthur C. Reber, Meichun Qian, Hector M. Saavedra, Paul S. Weiss, Shiv N. Khanna, and Ayusman Sen. Controlling Band Gap Energies in Cluster-Assembled Ionic Solids through Internal Electric Fields, ACS Nano (11 2010)
11/07/2008	18.00	M.A. Sobhy, J. Ulises Reveles, Ujjwal Gupta, S.N. Khanna, A.W. Castleman Jr.. Photoelectron Imaging and Theoretical Investigation of Bimetallic Bi1-2Ga0-2 and Lead Pb1-4 Cluster Anions, ( )
12/07/2010	48.00	Joshua J. Melko, S. Vincent Ong, Ujjwal Gupta, J. Ulises Reveles, Jonathan D'Emidio, Shiv N. Khanna, and A. W. Castleman, Jr.. Anion Photoelectron Spectroscopy and First-Principles Study of PbxIny Clusters, Journal of Physical Chemistry C (10 2010)
12/08/2010	49.00	Joshua J. Melko, S. Vincent Ong, Ujjwal Gupta, J. Ulises Reveles, Jonathan D'Emidio, Shiv N. Khanna, A.W. Castleman Jr.. Resilient aromaticity in lead–indium clusters, Chemical Physics Letters (10 2010)
12/11/2012	85.00	Cuneyt Berkdemir, C. L. Harmon, K. Don Dasitha Gunaratne, A. W. Castleman, Jr.. Probing the Valence Orbitals of Transition Metal-Silicon Diatomic Anions: ZrSi, NbSi, MoSi, PdSi and WSi, Phys. Chem. Chem. Phys. (11 2012)
TOTAL:	**36**	

Number of Manuscripts:

Books

Received	Paper

TOTAL:

Patents Submitted

Patents Awarded

Awards

Graduate Students

NAME	PERCENT_SUPPORTED	Discipline
Vince Ong	1.00	
M. Baddick	1.00	
Hua Zhang	0.50	
Chris Harmon	0.50	
Don Gunaratne	0.50	
Matt Ross	0.50	
Jordan Smith	0.50	
Eric Tyo	0.50	
FTE Equivalent:	**5.00**	
Total Number:	**8**	

Names of Post Doctorates

NAME	PERCENT_SUPPORTED
V. Medel	1.00
Meichun Qian	1.00
Matt Grochowski	1.00
Ran Liu	0.50
Debabrata Patra	0.50
S. Mandal	0.50
Zhi Luo	0.50
David Meenrajan	1.00
Shibo Cheng	0.50
Josh Melko	0.50
FTE Equivalent:	**7.00**
Total Number:	**10**

Names of Faculty Supported

NAME	PERCENT_SUPPORTED	National Academy Member
S. N. Khanna	0.25	No
A. Sen	0.25	No
A. W. Castleman, Jr.	0.25	Yes
FTE Equivalent:	**0.75**	
Total Number:	**3**	

Names of Under Graduate students supported

NAME	PERCENT_SUPPORTED	Discipline
Cameron Grover	0.50	Physics
FTE Equivalent:	**0.50**	
Total Number:	**1**	

Student Metrics

This section only applies to graduating undergraduates supported by this agreement in this reporting period

The number of undergraduates funded by this agreement who graduated during this period:	0.00
The number of undergraduates funded by this agreement who graduated during this period with a degree in science, mathematics, engineering, or technology fields:.....	0.00
The number of undergraduates funded by your agreement who graduated during this period and will continue to pursue a graduate or Ph.D. degree in science, mathematics, engineering, or technology fields:.....	0.00
Number of graduating undergraduates who achieved a 3.5 GPA to 4.0 (4.0 max scale):	0.00
Number of graduating undergraduates funded by a DoD funded Center of Excellence grant for Education, Research and Engineering:	0.00
The number of undergraduates funded by your agreement who graduated during this period and intend to work for the Department of Defense	0.00
The number of undergraduates funded by your agreement who graduated during this period and will receive scholarships or fellowships for further studies in science, mathematics, engineering or technology fields:	0.00

Names of Personnel receiving masters degrees

NAME
Total Number:

Names of personnel receiving PHDs

NAME
Eric Tyo
K. Don Dasitha Gunaratne
Matthew Ross
Total Number: 3

Names of other research staff

NAME	PERCENT_SUPPORTED
FTE Equivalent:	
Total Number:	

Sub Contractors (DD882)

Inventions (DD882)

Scientific Progress

Please see attachment.

Technology Transfer

I. ABSTRACT:

During the last couple of decades or so, the subject of nanoscale science began expanding into a unique field of science that offered the prospect of tailoring the design of materials having chosen properties. Two potentially promising approaches were conceived, one involving a bottom up approach while the other a top down method. In both cases, approaching the desirable nanoscale size regime where the properties of matter began to display nonlinear scalable behavior in which each atom counts, the connection to the area of cluster science began to be realized. Four well established academic groups (Castleman—PSU; Khanna---VCU; Sen---PSU; Weiss---PSU) successfully responded to a call for a MURI proposal with the eventual objective of expanding the concept of employing clusters and related superatoms for the use of building blocks for designing matter of nanoscale dimensions with tailored properties. The four groups, which had a history of closely interacting, fashioned a comprehensive research program to lay out the fundamentals for exploring the bottom up approach to design and produce new building blocks for several classes of systems including metals and alloys, metal compounds, metalloids, zintl ions and covalently bound species. Beyond the above, a major objective was to lay the foundation for producing materials with selected band gaps.

II. SUMMARY:

During the course of the five - year grant period (July 1, 2006 – June 30, 2012), we published 61 papers, which reported findings from a number of our collaborative activities. Regarding a study of the fundamentals of materials of building blocks, the Castleman group devoted attention to laying the foundation for producing and assembling superatom complexes that have tailored properties and appropriate stability; the Khanna group undertook requisite theoretical calculations related to structure, bonding and fundamental properties; the Sen group devised ways of extending the materials to the bulk state and/or the production of bulk amounts; characterization of the nanoscale materials was accomplished by the Weiss Group.

Considering that details of our numerous findings have been reported on a yearly basis, and already comprise a large number of scientific papers, this report gives a very brief overview of selected findings made during the grant period, mainly focusing attention on a few of the most important advances made. The prime objective of the program was to identify approaches to producing matter with well characterized superatoms having chosen properties and to tailored band gaps. Our initial and significant findings involved investigation of nanoscale species comprised of arsenic – alkali metal clusters, building on our prior work dealing with the analogous Bi - Na system. Early in our joint studies we succeeded in formulating protocols that enabled us to design and synthesize cluster-assembled materials composed of As_7 and As_{11} clusters in combination with alkali atoms; theoretical and experimental studies showed that the band gaps could be tuned by changing the alkali atom.

This early accomplishment served to establish the fundamental foundations needed for synthesizing the desired cluster building blocks and hence provided the impetuous for our subsequent detailed studies that involved identifying materials having unique electronic character. Controlling the assembly of multiply charged cluster building blocks into extended solids offers a strategy for constructing ionic cluster assembled materials with tunable properties. The As_7 cluster typically requires three additional electrons to complete its electronic shell. When combined with alkali metals, charge transfer from the alkali atoms to the As cluster follow the Zintl-Klemm concept and results in As_7^{3-} anions that are surrounded by alkali metal cations, thereby forming compact and crystalline cluster assemblies which have well defined band gap energy. These clusters were crystallized in the presence of the polycyclic multidentate ligand, 4,7,13,16,21,24-hexaoxa-1,10-diazabicyclo[8.8.8]hexacosane (commonly known as cryptand-222; henceforth "crypt"), and structurally characterized using X-ray crystallography. The selection of crypt as a cation sequestering agent facilitates the syntheses of Cs-linked cluster assemblies due to crypt's selective sequestering ability for K and Rb over Cs. Figure 1 shows an 8 cluster assembled material, with two examples each of 0-D, 1-D, 2-D, and 3-D cluster assemblies. The structures of all the clusters have been solved by using single crystal X-ray

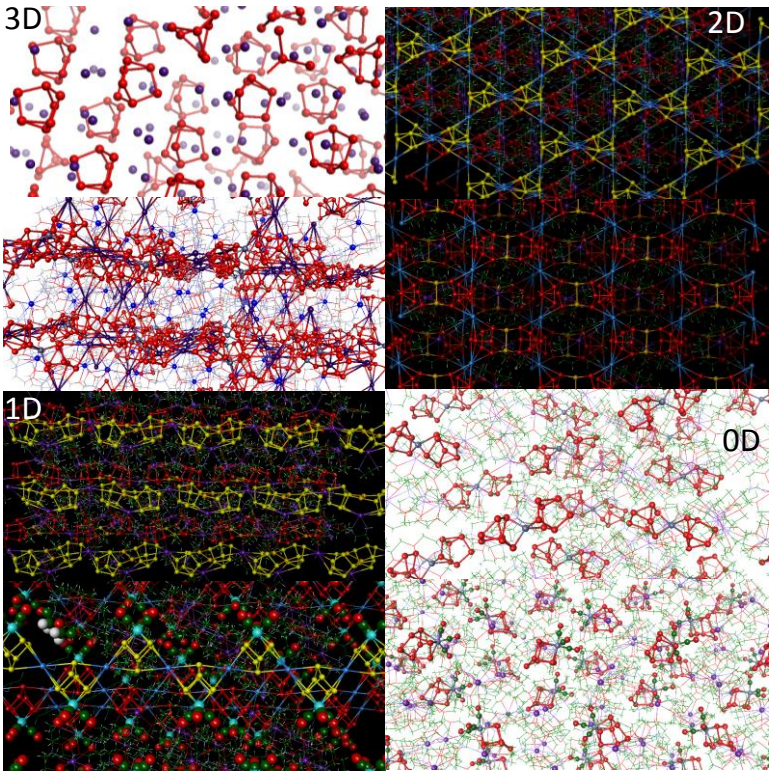

Figure 1. *Crystal structure of cluster assemblies with 3D architectures,* ***1****, and* ***14****, 2D architectures,* ***2****, and* ***7****, 1D architectures,* ***9****, and* ***23****, and 0D architectures* ***10****, and* ***18****.*

diffraction techniques. The judicious choice of the counterion, stoichiometry, and degree of cryptation offers several degrees of freedom which allow the construction of numerous cluster assembled materials with different properties.

Another achievement was the synthesis of $Te_2As_2^{-2}$, the first four-membered ring Zintl ion made from a combination of group 15 and 16 elements. And yet another notable finding was the formation of a one dimensional chain consisting of As_7 clusters linked by Au and K atoms. Again this work led to materials with band gaps which can be tuned over a wide range. New findings also have been made in effecting the formation of aluminum nanocrystals, and studies of aluminum-bismuth compositional materials have revealed the formation of compounds with band gap tuning capabilities and aromatic bonding structures. The latter feature opens up a new avenue to pursue in developing new superatom building blocks for cluster assembly.

The covalent linking of arsenic clusters into composite building blocks has also yielded variations in the band gap energy. We have synthesized dimer based cluster assemblies, and a theoretical description based on cluster orbital theory is used to provide a microscopic understanding of the electronic character of the composite building blocks and the observed variations in the band gap energy. We have also investigated cluster assemblies linked by Pd dimers which result in a valence state embedded in the band gap, and charge transfer complexes of $M(CO)_3$ which attach to the arsenic clusters.

More recent studies were made of a series of Si – transition metal species of interest in the field of electronic materials. Another major advance we made revealed that internal electric fields generated by counterions were able to modulate the band gaps of the assembled materials, which has helped us develop a novel protocol for developing band-gap-tunable materials.

Building on our efforts in the area of synthesis and characterization of cluster assemblies, we made numerous findings that have helped bridge the gap between gas-phase clusters and assembled materials of nano scale dimensions.

Within the gas-phase cluster characterization studies, we produced a class of heteroatomic gas-phase clusters that are analogous to the Zintl ion Sn_5^{2-}. These stable clusters, namely $Ga_2Bi_3^-$, $In_2Bi_3^-$, and $In_2Sb_3^-$, show promise for solution-phase synthesis, and our gas-phase work coupled with theory has revealed that the stability of these heteroatomic species is most enhanced when the atomic size mismatch between the constituent atoms is minimized. We have found that the chemical, electronic, and magnetic properties of clusters vary markedly with size and composition due to both quantum confinement and chemical interactions. In other work, we discovered the role of spin effects in oxidation and showed that aluminum and other clusters can be passivated by adding only a few hydrogen atoms.

During the course of the work we undertook the gas-phase characterization of other new cluster building blocks consisting of aromatic and closed shell species, clusters with similar electronic structures. We also studied a large range of lead-indium clusters with experiment and theory, showing that stable clusters can be governed in some cases by aromaticity while in others by filled electronic shells. The chemical bonding picture within these heavy-element clusters has also revealed that their stability may be more resilient than their light-element counterparts. Significantly, we have revealed that two heteroatomic clusters, which do not share any common elements, can possess similar electronic structures, providing for the possibility of replacing expensive building blocks with less expensive mimics. We have extended this idea from dimers up to four-atom clusters. Thereafter we studied a variety of transition metal silicides with photoelectron imaging, which has provided details of the electronic structure and chemical bonding picture. We have found that the chemical, electronic, and magnetic properties of clusters vary markedly with size and composition due to both quantum confinement and chemical interactions. The fundamental information gained reveals subtle interactions between transition metals and silicon, which is an important issue for spintronics applications.

In another investigation a variety of zinc oxide clusters were created and characterized in the gas phase, which revealed both subtle cluster growth patterns as well as a preferential stoichiometry (i.e. Zn_nO_{n+1}) that we propose to be considered for assembled zinc oxide materials. These studies revealed the effect that a transition metal atom can have on the band gap of the cluster assemblies, providing an additional degree of tunability. Through these studies we are beginning to develop a methodology for connecting the gas-phase reactivity of isolated clusters with changes incurred by deposition onto surfaces. As an extension of this work, we also investigated nanoclusters as a substrate for surface enhanced Raman spectroscopy. Both silver and gold nanoparticles were synthesized, whereupon we found that these species can greatly enhance and resolve Raman signal, a finding that could aid in the identification of components in a complex mixture.

In another phase of the program we investigated III-V cluster systems and identified a series of stable all-metal, neutral, aromatic clusters (Al_3Bi, Al_3Sb, Al_3As), as well as new superatom candidates (Al_5Bi, Al_5Sb, Al_5As), all of which possess large HOMO-LUMO gaps (1.12 – 1.86 eV). Further, our studies on bismuth-gallium clusters have elucidated a series of clusters with tunable band-gaps (from 1.12 – 1.89 eV).

These advances have been possible due to the open communication and close collaboration between all group members and PI's, which has greatly aided our ability to discover and develop new ideas. Further, we continued to hold our video conferences, which

were typically scheduled every two weeks. New ideas, results and research progress were presented in front of all groups. This synergistic format has contributed to a number of the accomplishments outlined herein.

III. Research Accomplishments for the current year (July 1, 2011 – June 30, 2012)

Prediction of stable Magnetic Superatoms

The concept of magnetic superatoms was formulated during the MURI program. To establish that assemblies of building blocks offer novel properties, we investigated transport through dimers of the magnetic superatoms (Cs_8V-Cs_8V) that are capable of almost 100% spin polarization , and magnetism in Fe chains decorating graphene edges. A central theme of the MURI was to demonstrate that cluster assembled nanoscale materials offer tunable properties. Taking band gap as the property of choice, we also participated in investigations on cluster assembled nanoscale materials including cluster assembled materials based on As_7^{3-}, As_{11}^{3-} building blocks where we demonstrated that the band gap could be varied by changing countercations, covalent linkers, or introducing states in gap, from about an 1.0 eV to 2.2 eV. We also developed assemblies based on ligated Ag_4Ni_2 clusters and aromatic building blocks that exhibit novel optical properties. Finally, we also collaborated with an experimental group outside the MURI team to provide insights into microscopic mechanisms for developing Cu and Ni nanoparticles by a polyol method. Our work on magnetic superatoms has attracted considerable attention by other scientists and the scientific news media.

Towards Magnetic Silicon-Based Semiconductors:

The current microelectronics industry relies heavily on the semiconducting material, silicon. Attaining an atomic level control over the synthesis and properties of silicon-based clusters and assembling them to create new cluster assembled materials will have technological implications. The biggest challenge is to find stable clusters that have interesting properties and yet are stable enough to retain their identity during their assembly to form cluster-assembled materials. It will be even more interesting if the new clusters could be magnetic because of the recent interest in magnetic semiconductors and spintronics devices with novel functionalities. Our work explored this later possibility through comprehensive investigation of the transition metal-silicon clusters, Si_nTM_2 (TM=Cr, Mn, $1 \leq n \leq 8$) containing two transition elements. The choice of Cr and Mn was motivated as the isolated Cr and Mn atoms have high spin moments of 6.0 μ_B and 5.0 μ_B respectively. Isolated Cr_2 and Mn_2 dimers are known to have anti-ferromagnetically aligned local spin moments. It was then interesting to examine if, along with stabilizing the atomic moments, the silicon clusters could also alter the magnetic coupling.

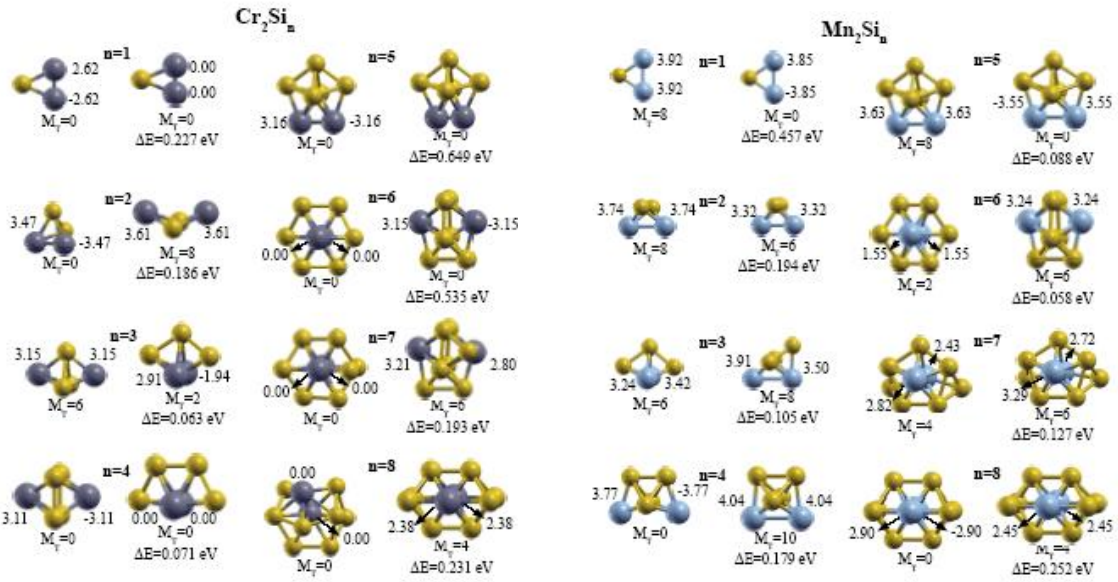

Fig. 1 Geometries and spin multiplicity of Si_nTM_2 (TM=Cr, Mn, 1≤n≤8) clusters.

In Fig. 1, we show our findings on Cr_2Si_n and Mn_2Si_n clusters containing up to 8 Si atoms. A study of the energetics brought out an interesting finding. Mn_2Si_4 was found to be a highly stable cluster with a large HOMO-LUMO gap. The cluster had antiferromagnetically coupled Mn atoms in the ground state but had a ferromagnetically coupled state only 0.18 eV higher in energy. We then investigated the magnetic configuration of a composite cluster composed of two units. What was surprising was that in most cases, the composite units had large spin moments. We are continuing with efforts to assemble these size-selected clusters in the new cluster deposition apparatus. This may allow us to finally be able to make silicon based spintronics devices through assemblies of these motifs.

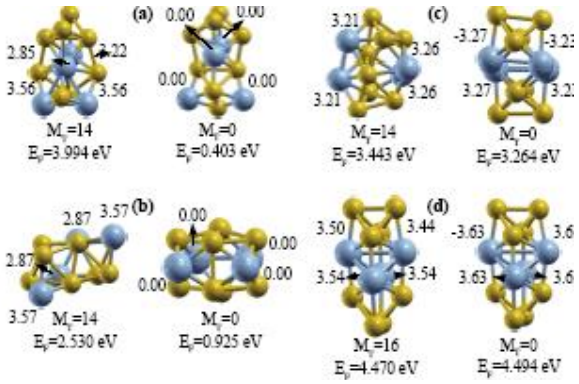

Fig. 2 Relaxed geometries of two Mn_2Si_4 clusters brought together starting from different initial configurations.

Magnetism in assembled and supported silicon endohedral cages

Transition metal encapsulated silicon cages are especially stable, but their use as building blocks of nanomaterials to be used in spintronics is limited by the quenching of the

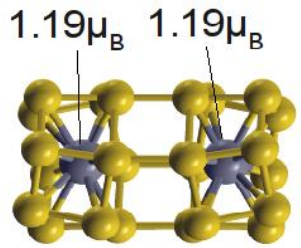

Fig. 3. Magnetic moment of a dimer of two Cr@Si12 Clusters.

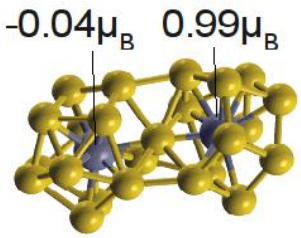

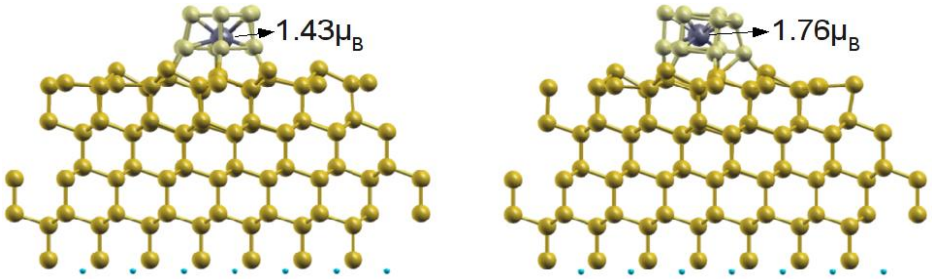

Fig. 4. Magnetic moment of a dimer Cr@Si12 Clusters on a Si surface.

magnetic moment. One example is the $Cr@Si_{12}$ cluster, which was previously studied in our group. This cluster presents a Cr atom encapsulated in a Si cage with a hexagonal bi-prism structure. The Cr magnetic moment is completely quenched due to the Cr-Si hybridization. By performing density functional calculations we have shown that the magnetic moment of this cluster can be recovered by bringing two of them together (Fig.3) or by depositing them on a silicon surface (Fig.4). In these two situations new Si-Si bonds are formed, weakening the Cr-Si bonds and recovering the local Cr magnetization. We can imagine that both effects could be combined by the random deposition of these highly stable motifs on a surface. That would enhance the transition magnetic moment and could be a feasible way of producing a magnetic silicon-based semiconductor material.

Magnetic Superatoms: Building Blocks of New Spintronics Devices:

Recently, we extended the superatom concept to "magnetic superatoms". The superatoms generally require filled electronic shells to acquire energetic stability whereas magnetism breeds through unpaired electrons. We have shown that these seemingly opposite requirements can be simultaneously fulfilled by taking a combination of localized atomic orbitals to breed magnetism and delocalized orbitals to stabilize the cluster through nearly free electron supershells. We showed that a cluster consisting of one V and eight Cs atoms is like a

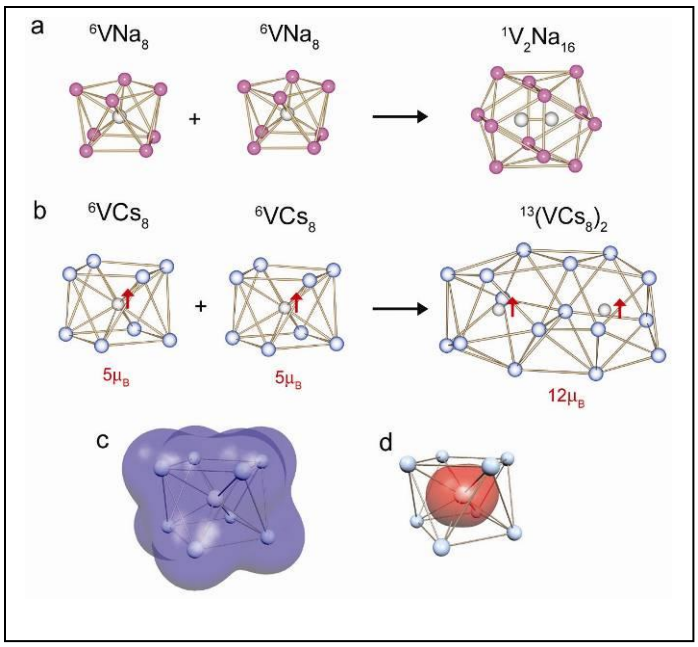

Fig. 5. Lowest energy structures of V_2Na_{16} and $(VCs_8)_2$ dimer. Total and net spin electron density of VCs_8. a, V_2Na_{16} and b, $(VCs_8)_2$ dimer starting from free clusters. The arrows indicate the direction of the V local spin moments. The superscripts indicate spin multiplicity. The total electron density c, and net spin electron density d (isoval = 0.001 a.u.), in a VCs_8 cluster. The spin density is mostly localized at the center around the V-site.

tiny magnet that can mimic a Mn atom in magnetic strength while acquiring stability through the delocalized electrons. Our findings that appeared in the journal Nature Chemistry have opened a new era in "magnetic superatoms", clusters that impersonate different elements of the periodic table.

Using first principles electronic structure methods, we examined the electronic structure and magnetic properties of clusters having one V surrounded by multiple Cs atoms. The results indicated that when the cluster had eight Cs atoms (Fig. 5), it acquired extra stability due to a filled electronic shell $1S^21P^6$ in a jellium framework. Further, the cluster had a spin magnetic moment of 5 Bohr magneton, more than twice of an iron atom. It is interesting to note that a Mn atom also has a similar magnetic moment and a closed electronic shell of more tightly bound atomic electrons. Hence, the cluster could be regarded as a mimic of the Mn atom. We also extended our studies to ligated clusters to demonstrate the applicability of the idea and showed that a ligated $MnAu_{24}(SH)_{18}$ is also a magnetic superatom.

It is worthy of note that our recent preliminary studies on transport of such superatoms in a dimer are predicting unusual spin polarization that could lead to potential applications in spintronics devices.

Highly efficient (Cs_8V) super-atom based spin-polarizer

As mentioned above, we had extended the superatom concept to include magnetic clusters called "magnetic superatoms". The superatoms generally require filled electronic shells to acquire energetic stability whereas the magnetism is acquired through localized electrons. We

proceeded to cover other magnetic clusters including alkali coated Sc and Ti clusters to propose newer magnetic superatoms.

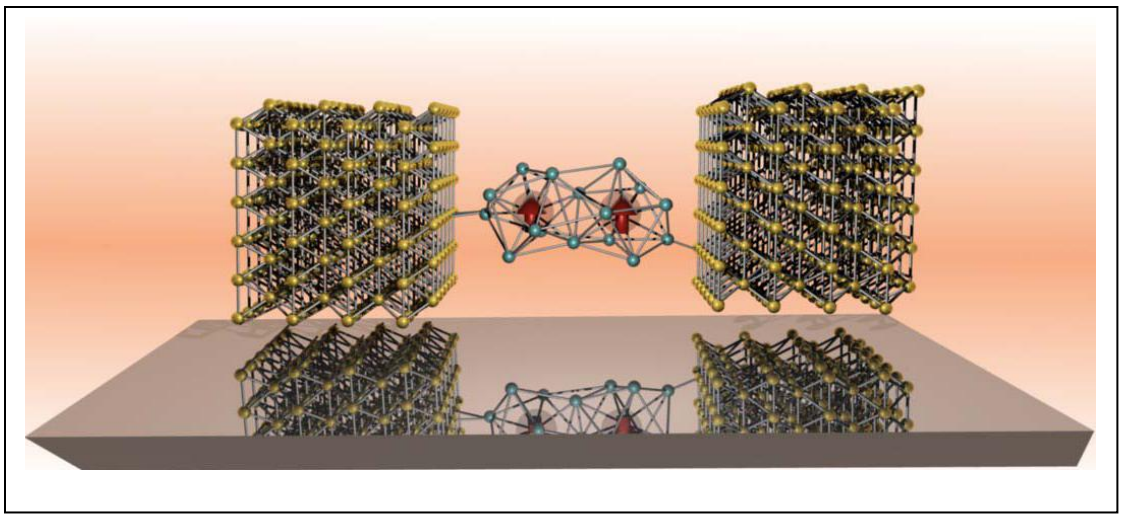

Fig. 6. A schematic representation of the superatom based model system Au-(Cs_8V)-(Cs_8V)-Au. Yellow, blue and red balls represent the Au, Cs, and V atoms respectively. The arrows indicate the direction of spin magnetic moments at the V sites.

An important question surrounding the magnetic superatom discovery pertains to the new features that are offered by such building blocks. Since quantum transport through molecules and the possibility to manipulate spin is suggested by the findings we proceeded to examine the spin transport through a molecule of magnetic superatoms (see Fig. 6).

A molecule composed of two Cs_8V magnetic superatoms was connected to two slabs of gold atoms and we carried out calculations of the current transport through such an assembly. Our calculations based on density functional theory and non-equilibrium Green's function methods find a much higher current for the spin-down charge carriers relative to the spin-up carriers in the model Au-(Cs_8V)-(Cs_8V)-Au device system with almost 100% spin polarization, indicating a highly efficient spin polarizer. The new behavior is rooted in strong coupling of the localized magnetic core on V and the itinerant electrons of the Cs leading to nearly full spin-polarization. This nearly-full spin polarization is comparable to that of the newly-developed half-metals (such as $La_{0.66}Sr_{0.33}MnO_3$ P=96% and CrO_2 P=98%) and significantly higher than the traditional ferromagnetic transition metals (such as Fe, Co, Ni P=40-50%) offering potential for applications.

Aromatic and Jellium Building Blocks in Al_nBi clusters for Nanostructure Materials

The family of Group III and Group V mixed species in the bulk form a variety of semiconducting materials. These states are well understood and described by band theory. However metal clusters of these groups which can vary in size and composition have a very different relationship between their geometry and electronic states. One such system is that of aluminum-bismuth clusters. Using the combination of density functional theory first principle calculations and negative ion photodetachment experiments and velocity map imaging we found that the electronic structure of two stable neutral clusters, Al_3Bi and Al_5Bi, can be explained using the aromatic and "Jellium" construct, respectively. The Al_3Bi cluster was found to have a

high ionization potential (7.08 eV), a low electron affinity (1.41 eV), and a very large gap (1.69 eV) between the highest occupied and lowest unoccupied molecular orbitals (HOMO-LUMO gap). This along with the gain in

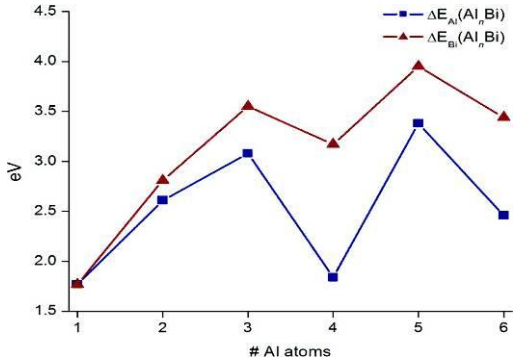

Figure 7. Calculated energy gain (in eV) for aluminum (ΔE_{Al}) and bismuth (ΔE_{Bi}) from the neutral Al_nBi clusters (n = 1-6).

energy as one adds Al atoms to the cluster for the Al_3Bi cluster (~3.2 eV) reveals this cluster is stable relative to its nearest neighbors (Figure 7). The stability was found to be rooted in the delocalization of electrons from the molecular orbital diagram and thus was determined to be that of aromaticity (Figure 8A). Even though the Al_5Bi has the highest gain in energy (~3.4 eV) of all the Al_nBi clusters (n = 1-6) and a HOMO-LUMO gap of 1.15 eV indicating its special stability, the explanation for its stable behavior is governed

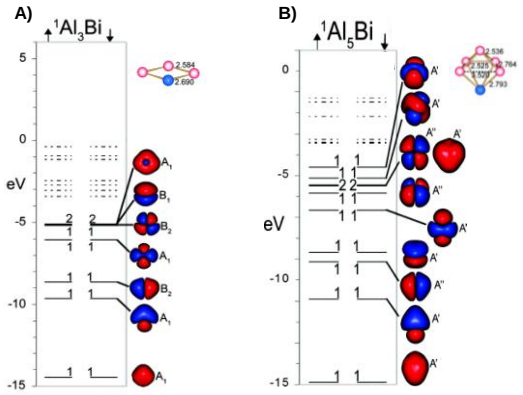

Figure 8: Molecular orbital diagrams with electronic states and molecular geometries of A) Al_3Bi and B) Al_5Bi clusters. The solid lines represent the occupied states and the dotted lines represent the unoccupied states. The bond lengths are given in Angstroms.

by a different model. The total number of electrons in the Al_5Bi cluster is 20, which results in the "Jellium" stable electron configuration $1S^2\ 1P^6\ 1D^{10}\ 2S^2$. Further analysis from the molecular orbital diagram of the Al_5Bi cluster shows that this is indeed the case (Figure 8B).

Cluster Assembled Material with Aromatic Building Motifs:

Aromaticity and antiaromaticity, once purely the domain of organic chemistry, has been expanded in recent years to include organometallic complexes, all-metal clusters, and main-

group compounds. In a valuable development, we succeeded in the synthesis and crystal structure of $Te_2As_2^{2-}$, the first four-membered ring Zintl anion made from a combination of group 15 and 16 elements. The planar anion, sandwiched between two potassium 18-crown-6 units, has alternating Te—As bond lengths and angles that give it a parallelogram geometry. Theoretical analysis of the structure and molecular orbital analyses revealed a quite unusual electronic structure for the anion: σ-antiaromatic bonding coupled with π-aromatic bonding and a triplet electronic ground state, which leads to the distorted square shape and net aromatic character. While similar systems with this "conflicting aromaticity" have previously been observed in the gas phase, $Te_2As_2^{2-}$ is the first example isolated as a solid (see Fig. 9).

In addition to aromaticity, one of the most unusual findings was that $As_2Te_2^{-2}$ has a triplet ground state. The resulting bulk also had a ferromagnetic ground state, suggesting a source of magnetism from assembly of non-magnetic solids.

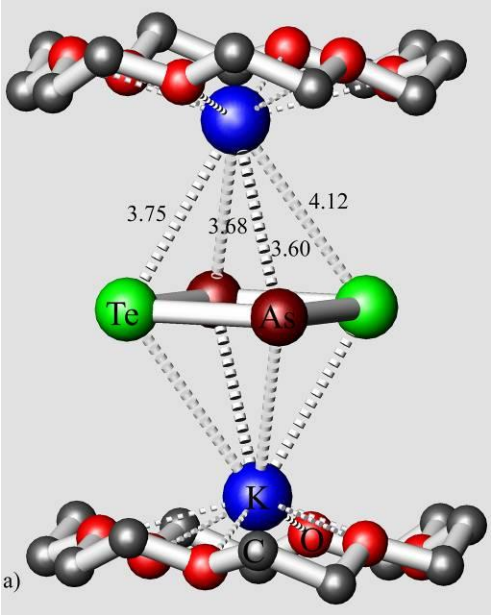

Fig. 9. Side view of [K(18-crown-6)]$_2$[Te_2As_2] cluster assembled solid.

New Building Blocks for Nanostructure Materials

In an effort to extend our search to new families of building blocks for cluster materials, we have carried out synergistic efforts combining experiments and theoretical work on a variety of systems. One of these involves the extension of the concept of aromaticity to three dimensions to show that it can play a role in the stabilizing deltahedral Zintl clusters. To show this, we studied Zintl analogues comprised of bismuth doped tin clusters with photoelectron spectroscopy and performed theoretical analysis.

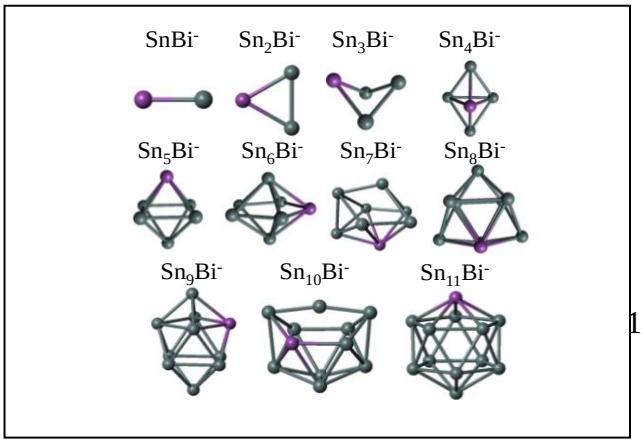

Fig. 10. Lowest energy structures for the $BiSn_n^-$ clusters (n = 1-11). The gray and pink spheres represent the tin and bismuth atoms, respectively.

To assign aromaticity, we examined the ring currents induced around the cage by using the Nucleus Independent Chemical Shift. We showed that a $BiSn_4^-$ cluster (Fig. 10) is stable and that its stability can be reconciled within aromatic criteria, while $BiSn_5^-$ is found to fit antiaromatic criteria and was shown to have reduced stability. The more stable clusters exhibit aromatic character which originates from weakly interacting *s*-states and bonding orbitals parallel to the surface of the cluster, while nonbonding lone pairs perpendicular to the surface lead to antiaromaticity and reduced stability.

An important class of semiconducting materials is one obtained by mixing Group III and Group V elements. However small clusters of these groups can exhibit new kind of bonding when combined in different proportion. For example, we just showed that In_2Bi^- and In_3Bi are both stable clusters where the origin of stability is rooted in the delocalization of electrons leading to an aromatic behavior (see Fig. 11). The stability

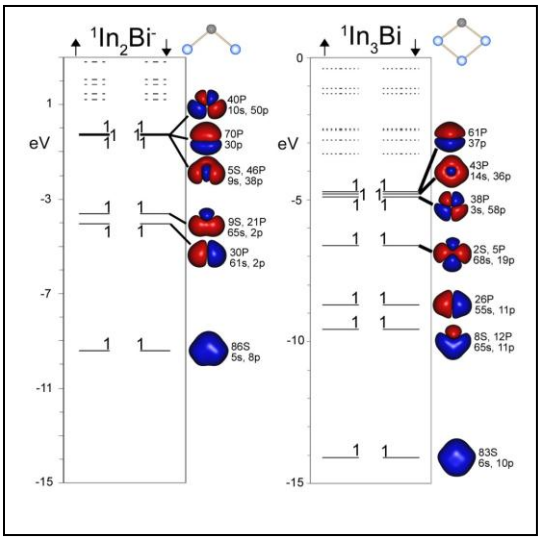

Figure 11. One electron energy levels and isosurfaces (isovalue = 0.03 a.u.) of the molecular orbitals for In_2Bi^- and In_3Bi. The continuous lines represent occupied levels, the dotted lines correspond to single unfilled states, the degeneracy is marked next to each level, and the arrows indicate the majority (up) and minority spin states. The atomic composition of each occupied orbital is also given.

results in a large HOMO-LUMO gap of 1.46 eV in In_2Bi^- and 1.34 eV in In_3Bi. The HOMO-LUMO gaps are comparable to 1.70 eV for a C_{60} cage and indicate that it should be possible to assemble these units into a cluster material.

New Building Blocks for Nanostructure Materials

In an effort to extend our search to new families of building blocks for cluster materials, we have carried out synergistic efforts combining experiments at PSU and the theoretical work at VCU on a variety of systems. One of these involves the extension of the concept of aromaticity to Pb_nIn_m and Bi_nSn_m clusters stabilized by aromaticity or filled electron shells. We also carried out studies on $Ga_nBi_m^-$, $In_nBi_m^-$, and $In_nSb_m^-$ clusters that are heteroatomic Zintl analogs of Sn_5^{2-} to examine the effect of atomic size on the stability. In the following we briefly outline our findings. We investigated the electronic structure and stability of three gas phase heteroatomic clusters, Ga_2Bi_3-, In_2Bi_3-, and In_2Sb_3-, which are isoelectronic with the Zintl ion Sn_5^{2-}, using photoelectron spectroscopy and first-principles theoretical investigations. While all the isoelectronic clusters are stable with high adiabatic detachment energies, the HOMO-LUMO gap, absolute stability and the relative stability of the isomers depend on the atomic size and point of substitution.

In another joint effort, we investigated the stability and electronic properties of anionic and neutral Pb_xIn_y clusters containing up to 5 Pb and up to 7 In atoms using negative ion photodetachment spectroscopy along with first-principles electronic structure studies within a gradient corrected density functional approach. Through studies of the detachment energies, gaps in the electronic spectrum, variations in binding energy, and nature of the electronic states, two families of stable

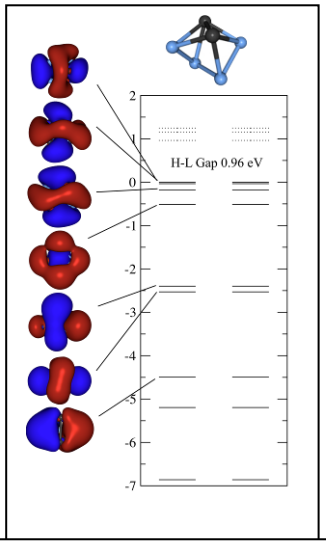

Fig. 12. One electron energy levels and isosurfaces (isovalue = 0.01 au) of the molecular orbitals for Pb_2In_4. The continuous lines are occupied states, the dashed lines represent unoccupied levels. The HOMO-LUMO gap is labeled as H-L gap.

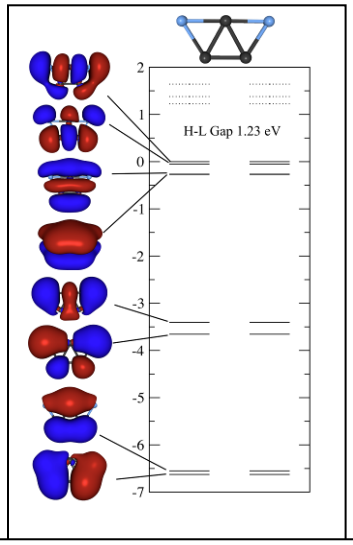

Fig. 13. One electron energy levels and isosurfaces (isovalue = 0.01 au) of the molecular orbitals for Pb_3In_2. The continuous lines are occupied states, the dashed lines represent unoccupied levels. The HOMO-LUMO gap is labeled as H-L gap.

species are identified. $PbIn_3^-$, Pb_2In_2, and Pb_3In_2 exhibit enhanced stability compared to their neighbors and the stability is linked to the aromatic character identified in their molecular orbitals. On the other hand, PbIn5- and Pb2In4 exhibit enhanced stability associated with filled electronic shells within a confined nearly free electron gas. In Fig. 12 we show the one electron energy levels in Pb_2In_4 with filled electronic shells in a confined nearly free electron gas model while Fig. 13 shows the energy levels and the associated orbitals in Pb_3In_2 that exhibits stability associated with aromatic character, the atomic size and point of substitution. Theoretical analysis reveals that the variations are attributable to atomic size differences, which affect covalent bonding within the cluster. The studies offer a strategy for controlling properties of clusters that might be incorporated into cluster-assembled materials. Fig. 14 shows the geometry and stability of the clusters.

Our studies indicate that although the heteroatomic clusters are singly charged, they all demonstrate enhanced stability as seen through the atomization energy and through the HOMO-LUMO gap. Further, the ground state geometry in all three cases is that in which the Group V atoms form an equatorial triangle, while the Group III atoms cap the trigonal bipyramid. This

enhances the bonding within the equatorial triangle, and only slightly weakens the bonding between the equatorial triangle and the capping atoms. However, differences in atomic size as one combines elements from differing periods does lead to variations in stability. This is evident as one examines the progression of the electronic structure as the identity of the atoms, and the position of substitution, is manipulated. Lastly, the stability of the heteroatomic cluster is maximized when the size mismatch is minimized as evidenced by enhanced stability of $In_2Sb_3^-$ versus the other five-atom clusters.

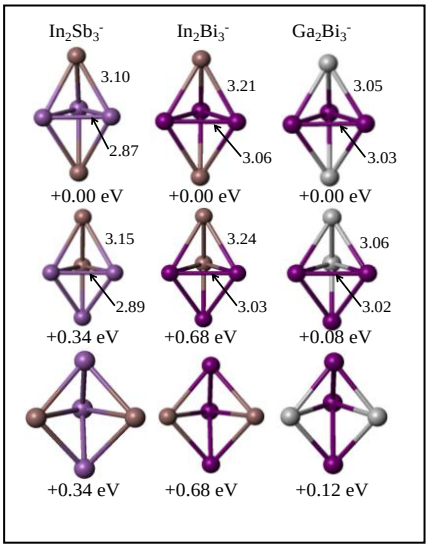

Fig. 14. The geometry, relative energy in eV, and bond lengths in Angstroms of $In_2Sb_3^-$, $In_2Bi_3^-$, and $Ga_2Bi_3^-$.

Controlling Magnetic coupling between Fe-chains by depositing at the edges of Graphene

The possibility of experimentally isolating single sheets of graphene and investigating the electronic, magnetic, optical, and chemical behavior of this two-dimensional arrangement of carbon atoms has generated considerable excitement. The single carbon sheet is a zero gap semiconductor, where the electrons behave like Dirac Fermions with linear energy dispersion and electron hole symmetry offering unusual transport properties. These include a display of quantum hall effect at room temperature, ballistic transport at sub-micrometer scale, and finite conductivity at zero carrier concentrations. These novel features are accompanied by developments in experimental techniques allowing fabrication of graphene based nanostructures including ribbons, dots and graphene molecules and clusters. One of the properties that have drawn considerable attention is the possibility of localized magnetic moments associated with edges in graphene-based nano-ribbon. While bulk graphite is diamagnetic, the electron-electron interaction can stabilize magnetic moments. For example, in nano-ribbons with zigzag edges, there is a large density of states at the Fermi energy due to states localized at the edges and this can lead to a magnetic instability in nanostructure. To examine if graphene nanoribbons could be used to mediate coupling between ferromagnetic (FM) materials, we examined the stability and coupling in Fe-chains at the two edges of a nano-ribbon. Figure 15 shows the ground state configuration of Fe-chains at the two edges. We find that the Fe-sites in each chain undergo a structural rearrangement into a chain of Fe2 dimers (Fe-Fe spacing 2.16 Å) separated by 2.77 Å.

The Fe-sites within a chain are ferromagnetically aligned with a spin moment of 2.3 μB per atom, but the chains across the ribbon have antiferromagnetic ground states mediated by the nano-ribbon. Studies on ribbons of increasing width show that the difference between the AFM

and FM configurations, decreases with increasing width, attaining a value of 8.9 meV per unit cell for chains separated by 2 nm. More interestingly, the states at the Fermi energy in the FM case are composed of only minority electrons offering the potential to generate spin-polarized currents by stabilizing FM state via applied magnetic fields.

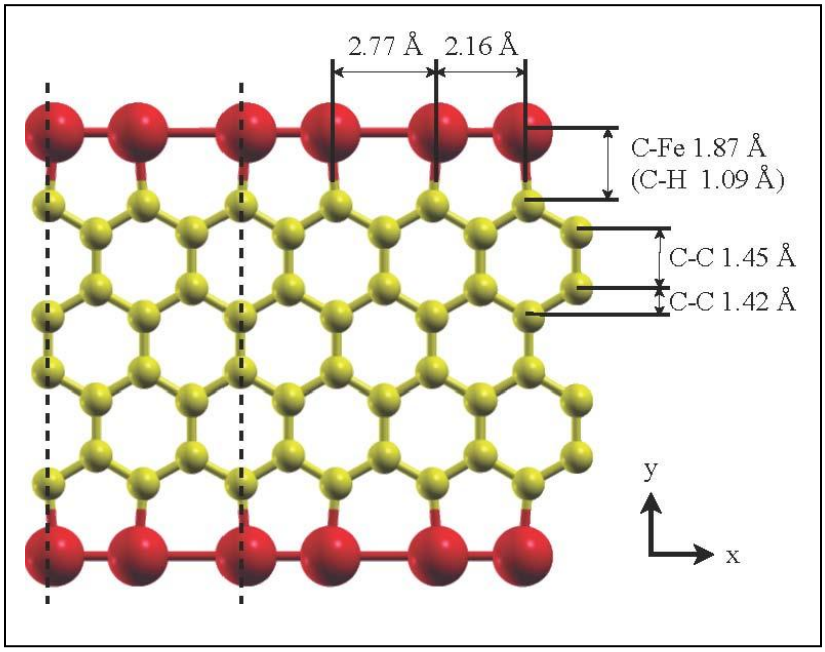

Fig. 15. Ground state of Fe-chain (red atoms) at the edges of a graphene nano-ribbon.

Cluster-assembled Materials: Preparation of Cu and Ni nanoparticles by Polyol Method.

As part of a collaboration with an experimental group at VCU, we participated in a comprehensive study involving the relationship between synthesis conditions, crystal morphology, and theoretical modeling of copper and nickel nanoparticles prepared by a modified polyol process. The polyol serves as a solvent, a reducing agent, and a capping agent and we investigated the role several polyol types play in the nucleation and growth of metallic nanoparticles. The nanoparticles were characterized by transmission electron microscopy (TEM), x-ray diffraction (XRD), and x-ray photoelectron spectroscopy (XPS). Our results demonstrate that changing the solvent system from a short chain polyol (ethylene glycol) to a long chain polyol (tetraethylene glycol) greatly affects the resulting morphology of copper nanoparticles. These results suggest that the polyol is playing a major role as an in-situ capping agent and that the various polyol chain lengths in-turn result in various particle morphologies by directly altering the nucleation and growth steps. Theoretical modeling in our group provided insight into the mechanism for growth to better understand the intermediate structure stability. This work presents an alternative approach in investigating the polyol mechanism by using both theoretical and experimental results and opens new insight for the synthesis of metals and alloys by the polyol process.

Determination of Band Gap Energy:
The variations in the composition and architecture of cluster assemblies constructed from the same building block result in different electronic, and optical properties. We demonstrated this by measuring the optical band gap energy of 23 cluster assembled materials based on As_7 that we have synthesized, using diffuse reflectance spectroscopy, and the Kubelka-Munk model. This two-flux model, which considers only diffuse light, is generally used to determine the absorption coefficients from a surface that both scatters and absorbs incident radiation. For a crystalline solid with a nonzero band gap energy (E_{bg}), the frequency dependence (ν) of the absorption coefficient (κ) can be approximated as:

$$\kappa(\nu) = \frac{B_T(h\nu - E_{bg})^n}{h\nu},$$

where B_T is a constant derived from the square of the averaged dipolar momentum matrix element, and n is equal to 0.5 and 2 for *direct* and *indirect* band gap transitions, respectively. The absorption coefficient (κ) can be measured from the reflectance (R) and expressed as $\kappa = (1-R)^2/2R$. Using the above equation, the band gap of a material can be obtained by extrapolating to the x-axis intercept with a linear fit to a plot of $(\kappa h\nu)^{1/n}$ *vs.* $h\nu$. Figure 16A shows these Tauc plots for the measured cluster assemblies of **1**-**4**, while the values of the band gap energies for all the mentioned cluster assemblies are listed in Table 1. The formula for indirect band gap energy was used in all cases as we have found this to be most appropriate for these systems with rather flat bands.

Table 1. Experimentally measured and theoretically calculated band gap energy for all clusters.

Comp.	**Cluster Formula**	**Band-gap (eV) (Exp.)**	**Band-gap (eV) (Theor.)**
1	$[Cs_3][As_7]$	1.09±0.052	*1.19*
2	$[(K\text{-}Crypt)Cs_2][As_7]$	2.04±0.17	*1.98*
3	$[(K\text{-}Crypt)_{1.5}Cs_{1.5}][As_7]$	2.08±0.05	*1.84*
4	$[(Rb\text{-}Crypt)_{1.5}Cs_{1.5}][As_7]$	1.77±0.05	*1.80*
5	$[K\text{-}Crypt]_4[Au_2(As_7)_2]$	1.69±0.02	*1.68*
6	$[(Rb\text{-}Crypt)Rb_2]_2[Au_2(As_7)_2]$	1.87±0.05	2.09
7	$[(K\text{-}Crypt)_2Cs_2][Au_2(As_7)_2]$	1.97±0.01	2.06
8	$[(Rb\text{-}Crypt)_2Cs_2][Au_2(As_7)_2]$	1.98±0.05	2.00
9	$[(K\text{-}Crypt)_2K_2][Au_2(As_7)_2]$	1.46±0.02	1.43
10	$[K\text{-}Crypt]_4[Zn(As_7)_2]$	1.99±0.05	*1.97*
11	$[K\text{-}Crypt]_4[Cd(As_7)_2]$	1.87±0.04	*1.92*
12	$[K\text{-}Crypt]_4[Hg_2(As_7)_2]$	1.67±0.04	*1.72*
13	$[K\text{-}Crypt]_3[HgAs(As_7)_2]$	1.62±0.04	*1.59*
14	$[K\text{-}crypt]_2[Zn(As_7)_2Cs_2]$	2.16±0.02	*1.96*
15	$[K\text{-}crypt]_2[Cd(As_7)_2Rb_2]$	2.21±0.04	*1.96*
16	$[K\text{-}crypt]_4[Pd_2(As_7)_2]$	1.35±0.003	1.39
17	$[K\text{-}crypt]_2[Pd_2(As_7)_2Cs_2]$	1.15±0.004	1.14
18	$[K\text{-}crypt]_3[Cr(CO)_3As_7]$	1.80±0.003	2.10
19	$[K\text{-}crypt]_3[(en)Mo(CO)_3As_7Mo(CO)_3]$	1.64±0.004	1.70

20	$[K\text{-crypt}]_3[(en)W(CO)_3As_7W(CO)_3]$	1.52±0.004	1.65
21	$[K\text{-crypt}]_2[As_7Cr(CO)_3Cs]$	1.90±0.02	1.97
22	$[K\text{-crypt}]_2[As_7Mo(CO)_3Cs]$	1.76±0.02	1.89
23	$[K\text{-crypt}]_2[As_7W(CO)_3Cs]$	1.78±0.02	1.86

Band Gap Energy Tuning: Role of Countercation

We observed significant variations in the band gap energies of cluster-assembled materials constructed from the same As_7 cluster building block. For example, $[Cs_3][As_7]$ (compound **1,** Figure 1, 3D) has E_{bg} = 1.09 eV, while $[Cs_2(K\text{-Crypt})][As_7]$ (compound **2,** Figure 1, 2D) has E_{bg} = 2.04 eV. The experimental results also reveal general trends regarding the band gap energy in these cluster-assembled materials. For example, the two-dimensional sheets, $[Cs_{1.5}(K\text{-Crypt})_{1.5}][As_7]$ (compound **3**) and $[Cs_2(K\text{-Crypt})][As_7]$ (compound **2**), have larger band gap energy, E_{bg} = 2.08 and 2.04 eV, respectively, while the three-dimensional assembly, $[Cs_3][As_7]$ (compound **1**), has a lower band gap, E_{bg} = 1.09 eV. Cluster assemblies made from the same motif should be isoelectronic, yet the band gap is almost doubled on replacing Cs with cryptated K. First principles electronic structure investigations were undertaken to probe the electronic band structure and the nature of the electronic states marking the set of highest occupied and lowest unoccupied molecular orbitals (HOMO and LUMO, respectively). All calculations were carried out within a gradient corrected density functional formalism with two complementary schemes. The calculations on periodic solids were carried out using a plane-wave basis set with the projector augmented plane-wave method, while some representative clusters were studied using a real space linear combination of atomic orbitals molecular orbital approach to investigate local effects. The calculations on the bulk solids have been performed on the basis of X-ray crystallographic structures (Figure 16).

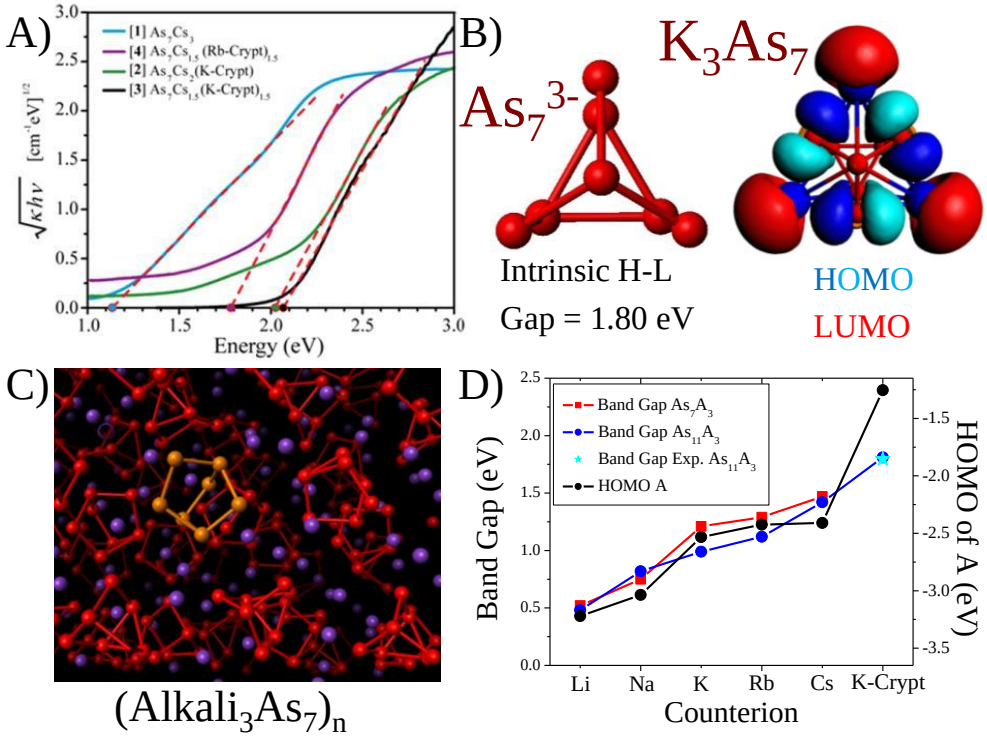

***Figure 16**. A) Tauc plots of **1**, **2**, **3**, and **4**. B) Structure of As_7^{3-}, and K_3As_7, with frontier orbitals for K_3As_7. C) Three-dimensional material for $[Cs_3][As_7]$ (compound **1**). D) Calculated band gap energy for A_3As_7 and A_3As_{11} Zintl phases in the crystal structure of 1C, and the absolute position of the HOMOs of the neutral atoms.*

To probe the origins of the variation in the band gap energies, we examined the nature of the frontier orbitals in isolated A_3As_7 clusters. The HOMO and LUMO charge densities are plotted in Figure 16b. The HOMO is composed of contributions from the As atoms, and the LUMO is localized on the alkali metal cations. This indicates that the orbital on the countercation and not the electronic structure of the As cluster building block primarily controls the position of the LUMO. The LUMO of the material is therefore derived from the absolute position of the HOMO of the neutral alkali metal atom. This close correlation is seen in Figure 16d, which shows the energies of the HOMOs of the alkali metal atoms and the calculated band gap energy of the pure Zintl materials. These were obtained by calculating the band structures of optimized A_3As_7 and A_3As_{11} assemblies for various alkali atoms in the observed orthorhombic and monoclinic structures of Cs_3As_7 and Cs_3As_{11}. The experimental and theoretical band gap energy for $[K\text{-}Crypt]_3[As_{11}]$ are also included, because $[K\text{-}Crypt]_3[As_7]$ cannot be crystallized. The HOMO of the free neutral atom is lowest for lithium and increases as the size of the atom increases, except for the cryptated potassium in which the lone pair on the polyether greatly destabilizes the HOMO. There is mixing of the states in solids with mixed countercations, as replacing a single Cs atom with cryptated K ions results in an increase of E_{bg} from 1.1 to 2.1 eV; so, the composition of the countercation is the dominant feature, which controls the band gap energy in these alkali metal linked Zintl clusters-assemblies.

Band Gap Energy Tuning: Role of Internal Electric Field

We synthesized multiple counterion directed architectures of $[As_7Au_2As_7]^{4-}$ as $[K\text{-}Crypt]_4[Au_2(As_7)_2]$, (compound **5)**; $[(Rb\text{-}Crypt)Rb_2]_2[Au_2(As_7)_2]$, (compound **6)**; $[(K\text{-}Crypt)Cs_2]_2[Au_2(As_7)_2]$, (compound **7)** and $[(Rb\text{-}Crypt)Cs_2]_2[Au_2(As_7)_2]$, (compound **8)**. X-ray crystallographic analysis reveal that all these compounds 5-9 have the same basic building $[As_7Au_2As_7]^{4-}$, but changing the cation results in zero- (**5**), and two-dimensional (**6**-**8**) architectures (Figure 17). The $[Au_2(As_7)_2]^{4-}$ units are arranged in a zero dimensional fashion in **5,** where none of these clusters interact with another. The experimental band gap energy of this material is found to be 1.69 eV and is in good agreement with the theoretically calculated value of 1.68 eV (Table 1). In this solid, the top of the valence band and bottom of the conduction band consist of As and Au states, respectively, as the K-Crypt states are pushed up and buried deep into the conduction band. The zero-dimensional solid compound **5** has the intrinsic band gap energy of an isolated $[Au_2(As_7)_2]^{4-}$ motif and can be used to guide understanding of the band gap energies in assemblies with higher connectivity. The structures of **6**-**8** are two-dimensional layers formed by interactions of naked Rb (**6**) and Cs (**7** and **8**) with $[Au_2(As_7)_2]^{4-}$, while cryptated alkali cations separate these layers (Figure 17b). The band gap energies of compounds **6**-**8** are found to be 1.87, 1.97, and 1.98 eV, respectively, and are in good agreement with the theoretically calculated values of 2.09, 2.06, and 2.00 eV for **6**-**8**, respectively (Table 1). Comparable values of band gap energies are expected for compounds **6**-**8** due to similar architecture. The striking result is that the band gap energies for all of the two-dimensional assemblies (**6**-**8**) are larger than the band gap energy of the zero-dimensional assembly (**5**), whose band gap energy is expected to be the upper limit. How then does varying the architecture

of the assembly increase the band gap energy to a larger value than that of an isolated cluster motif? We first consider the effect of architectural change on different interactions that the clusters may experience. In conventional solids, moving from a lower to a higher dimensional structure results in broadening of the valence and conduction bands, resulting in a smaller gap. Here, the band widths of the cesium linked (**7**) ionic cluster solids is 0.14 eV, so broadening does not significantly affect the band gap energy. The small band widths are due to weak direct overlap of electronic states in neighboring clusters as they are separated by cations. Changing the dimensionality of the ionic clusters assemblies, however, will change the long-range structure of the lattice and vary the depth of the electrostatic potential. The Madelung constant of the solid may also affect the total stability of the assembly, but it would not affect the band gap energy. Long-range electronic interactions act like a Faraday cage, where changing the depth of the potential shifts all electronic states equally and thus leaves the band gap energy unaffected. A significant local gradient in the electrostatic potential near the cluster, which modulates the electronic structure of the individual motifs, could be responsible for the unexpected band gap energy increase for the two dimensional cluster solids. We hypothesize that the counterions that are adjacent to the clusters generate an electric field that can significantly alter the local gradient of the electrostatic potential near the cluster motif. To demonstrate this, we calculated the electronic structure for an isolated $[Au_2(As_7)_2]^{4-}$ cluster (Figure 18a) with four point charges, *z*, placed at the same positions as Cs in the solid. The strength of the positive charges was varied from 0.0 to +1.0e, and we monitored the variation of the HOMO-LUMO gap as well as the location of the HOMO and LUMO. The gaps were found to increase smoothly by 0.34 eV when varying the point charge from 0 to +0.5e and then to decrease with higher fields. We found that the increase in the HOMO-LUMO gap is caused by the stabilization of the HOMO with the increasing field, while the LUMO states show little change until z = +0.6 e. Further increased electric fields reduce the gap as the As-Au mixed states are strongly stabilized to become the LUMO at high field. Similar electric field-dependent behavior is also observed for the case of As_7^{3-} clusters, however the gap increases monotonically from z = 0.0 to +1.0 e (Figure 18b). These results show that the band gap energies of the two-dimensional ionic solids, (**6**-**8**) increase due to the generation of internal electric fields by the adjacent counterions. We also examined the local electrostatic environment of other architectures to show that the internal electric fields are responsible for the increases of the band gap energy in materials **6**-**8**. Figure 18c shows the electrostatic potential of $[(Au_2)(As_7)_2]^{4-}$ and $Cs_4[(Au_2)(As_7)_2]$ as the models for **5** and **7**, respectively, on a plane cut parallel to the Au-As bonds with the associated HOMO plotted as an isosurface. An electric field corresponds to the gradient of the electrostatic potential, so a red to blue sequence indicates a stronger electric field. In $[(Au_2)(As_7)_2]^{4-}$, the electrostatic potential falls off gradually from the isolated cluster because no adjacent counterions are present to generate internal electric fields. In sharp contrast, for the case of $Cs_4[(Au_2)(As_7)_2]$, there is a large electric field generated by the Cs counterions, precisely along the path of the HOMO orbital. Since, the HOMOs generally protrude from the clusters, it is expected that an electric field will generally increase the band gap energy. The band gap energy variation also depends on the precise location of the electric field generated by the counterion and by the charge density of the states near the Fermi energy, so it may not always result in an increase of the band gap energy. Nevertheless, the variation of the electrostatic potentials shows that the band gap energy depends on the local electronic structure and the precise location of the counterions that generate the internal electric field, much like in cluster crystal-field theory.

(17A)

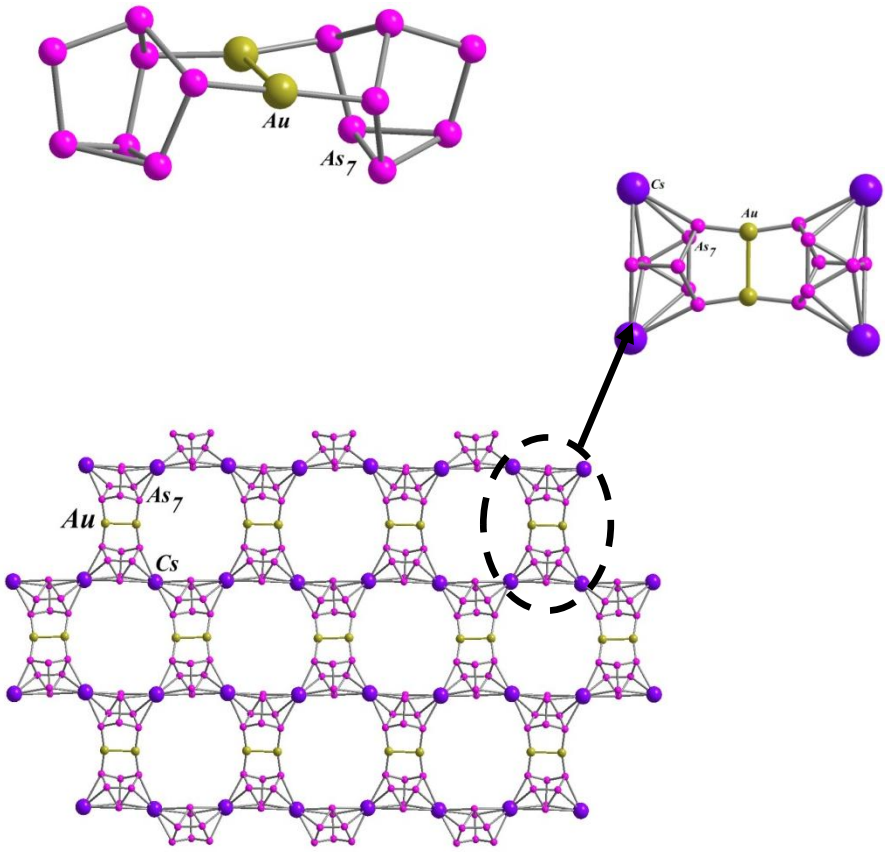

(17B)

Figure 17. (a) $[Au_2(As_7)_2]^{4-}$, two arsenic clusters are linked through a gold dimer in **5**. (b) Two-dimensional distorted honeycomb-like layers of $[Au_2(As_7)_2]^{4-}$ linked by Cs^+ in **7** as viewed along the a axis.

(a)

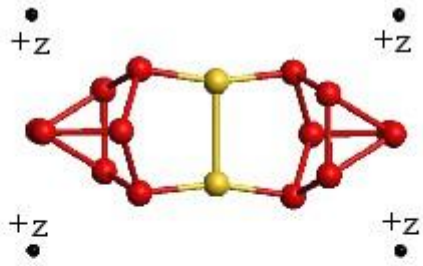

(b)

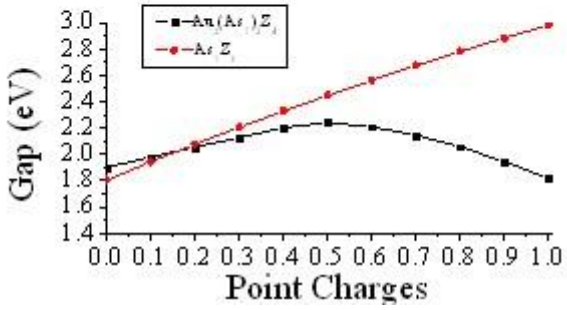

(c)

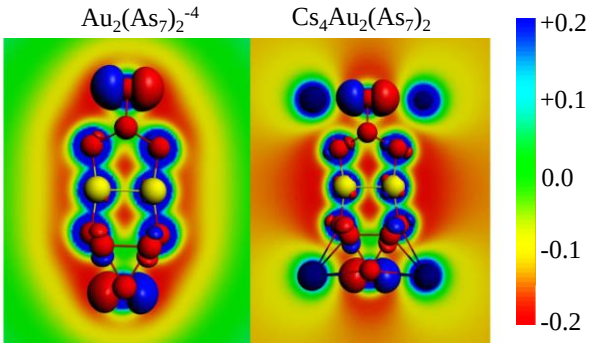

Figure 18*. (a) The positions of point charges in the cluster model, (b) variation of the band gap energies. The shifts are relative to the 5s core state of Au. (c) The calculated electrostatic potential of* $(As_7)_2Au_2^{4-}$ *and* $Cs_4(As_7)_2Au_2$ *(**5** and **7**). The potentials are shifted by 0.37 because of different total charges.*

Band Gap Energy Tuning: Role of Covalent Effect

We have synthesized a series of cluster assembled materials in which the building blocks are As_7^{3-} clusters linked by group 12 metals, Zn, Cd and Hg, to investigate the effect of covalent linkers on the band gap energy. The synthesized assemblies include zero dimensional assemblies of $[Zn(As_7)_2]^{4-}$, (compound **10)**, $[Cd(As_7)_2]^{4-}$, (compound **11)**, $[Hg_2(As_7)_2]^{4-}$, (compound **12),**. and $[HgAsAs_{14}]^{3-}$, (compound **13)**, (Figure 19) in which the clusters are separated by cryptated counterions. The Zn and Cd atoms covalently link the two As_7 clusters and the unit's electronic structure is mediated by the bonding between the clusters and the atom. The band gap energy was measured to be 1.99 ± 0.05 eV for the zinc-linked $[K\text{-Crypt}]_4[Zn(As_7)_2]\cdot 2en$, (compound **10)**, and 1.87 ± 0.04 eV for the cadmium-linked $[K\text{-Crypt}]_4[Cd(As_7)_2]\cdot en$, (compound **11**) (Table 1). An isolated As_7^{3-} cluster has a HOMO-LUMO gap energy of 1.80 eV, which demonstrates that the post-transition metal linker atoms increase the band gap energy. Since these cluster solids have cryptated K^+ as the counter ions, the increase in the band gap energy could be ascribed to the changes in the electronic structure as the two As_7 clusters are covalently coupled. In addition to band gap energy changes, the oxidation states of the composite clusters are -4 while the individual As_7 units have an oxidation state of 3-. To understand the progressions in the band gap energy, we first examine the nature of electronic spectrum as an individual As_7 cluster is first coupled with a Zn atom and then with another As_7 unit. The calculated electronic gap of 1.97 eV is close to the experimental value of 1.99 ± 0.05 eV. The molecular orbital diagram of Cd-linked As_7 is qualitatively the same as that of the Zn-coupled motif. The band gap energy of the Cd-linked clusters is 0.12 eV lower than that of the Zn-linked clusters. The density of states of the Cd- and Zn-linked clusters are shown in Figure 20, and they are essentially identical, confirming that the small difference in the band gap energy is not related to the bonding. The local charges on the Zn- and Cd- linked assemblies are both +0.46 e^-, so differences in electronegativity are unlikely to be the origin of the different band gap energies. Since the Zn and Cd assemblies have different space groups, it is possible that the differences are related to the structures. To explore this possibility, we calculated the band structures of the solids using the VASP code. The resulting densities of states (DOS) are shown in Figure 20b and the calculated band gap energy is 1.92 eV, slightly smaller than that of the Zn compound. A closer examination reveals that the minor difference is related to the change in unoccupied band

edge, indicating that the different packing of the crypt counterions has a small effect on the band gap energy.

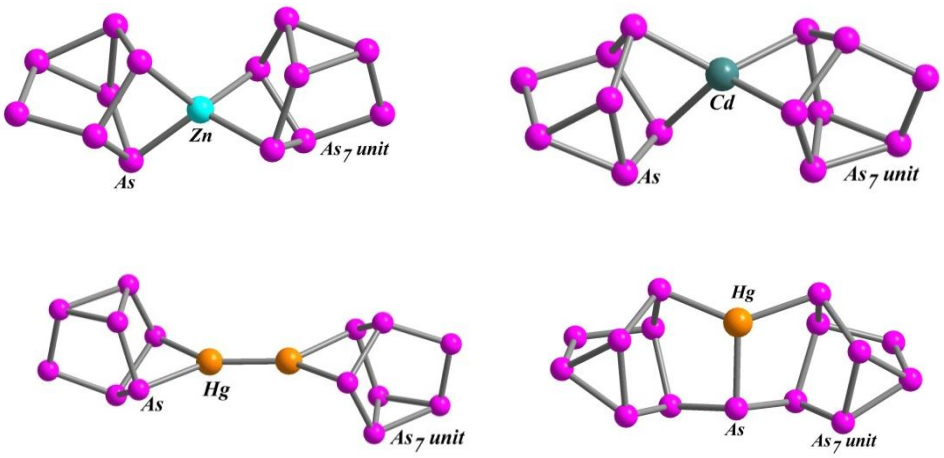

Figure 19. Cluster unit of a) $[K\text{-}Crypt]_4[Zn(As_7)_2]\cdot 2en$, **10**; b) $[K\text{-}Crypt]_4[Cd(As_7)_2]\cdot en$, **11**; c) $[K\text{-}Crypt]_4[Hg_2(As_7)_2]$, **12**; d) $[K\text{-}Crypt]_3[HgAsAs_{14}]$, **13**,. For clarity, [K-crypt] and solvent molecules are not shown.

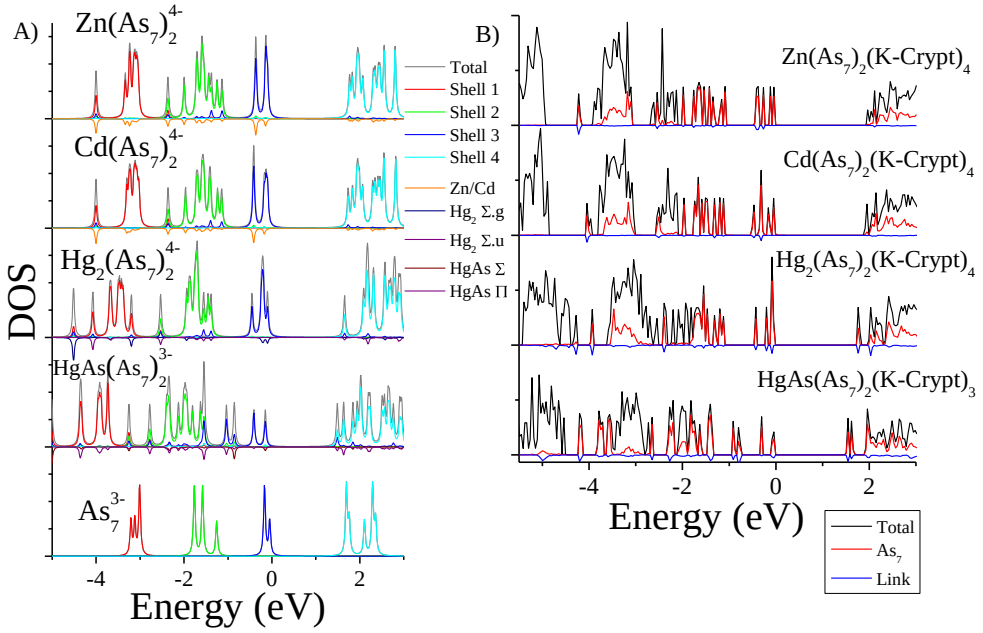

Figure 20. a) The density of states of the cluster models for **10–13** and As_7^{3-}. Shells 1-4 represent the projected density of states to the cluster molecular orbitals, which are closely grouped on As_7^{3-}. The negatively plotted states are projected from the HgAs molecule, which links the clusters. The DOS is positive, they are simply plotted negatively to guide the eye. b) The density of states of the periodic calculations for **10–13**. Black indicates total density of states, red indicates As_7 states, blue indicates the linker states, and the remaining states are attributed to the crypt.

Next we examine the molecular orbital diagram of $[Hg_2(As_7)_2]^{4-}$, (compound **12**). The Hg dimer is a weakly bound van der Waals molecule in which the valence 6s electrons form bonding and antibonding orbitals with a net bond order of zero. Hg_2^{2+} has a bond order of one, because the antibonding orbital is no longer filled. In the case of compound **12**, the 6s orbital of the Hg atom overlaps with the same *e* HOMO-1 orbital (Figure 21a) of the As_7^{3-} cluster near the Fermi energy as the Zn atom does, to form the molecular orbital shown in Figure 21c. The $[HgAs_7]^{3-}$ orbitals form bonding (Figure 21e) and antibonding orbitals (Figure 21h) when combined, and the antibonding orbital is unfilled resulting in a net bond order of one and a calculated bonding energy of 1.32 eV. Compound **12** is found to have a smaller band gap energy than that of **10** or **11**. This is caused by the splitting of the LUMO level of the $[Hg(As_7)]^{3-}$ intermediate, shown in Figure 21d into a pair of weakly bonding and antibonding orbitals (Figure 21f and Figure 21g). The LUMO in Figure 21h is stabilized in a weak bonding orbital, reducing the HOMO-LUMO gap energy of the solid. The $[Hg_2(As_7)_2]^{4-}$ is stabilized through oxidative coupling between the cluster-mercury complex, which pushes up the sigma antibonding orbital to reduce the oxidation state by two. The cluster orbitals of As_7^{3-}, which interact with the Zn and Cd atoms are the same orbitals that interact with the Hg atom, and the σ and σ* orbitals in the dimer complex are nearly perfect matches with the parent cluster orbitals. The formation of the $[Hg_2(As_7)_2]^{4-}$ complex through oxidative coupling conforms to the expectations of a "cluster orbital" theory in which the mixing of cluster orbitals behave much like bonding between atomic orbitals. The measured band gap energy of this compound is 1.67 ± 0.04 eV, (Table 1), approximately 0.32 eV lower than that for compound **10**. To probe the nature of the states marking the occupied and unoccupied bands in the solid, we calculated the band structure of the periodic structure, and the resulting DOS are shown in Figure 20b. Note that unlike compounds **10** and **11**, where the unoccupied band is formed by the electronic states of the crypt, the unoccupied band here is marked by states having significant contributions from the Hg and As_7 cluster orbitals. $[HgAs(As_7)_2]^{3-}$, compound **13**, was measured to have a band gap of 1.62 ± 0.04 eV, (Table 1), which is lower than the other covalently linked clusters due to larger broadening of the cluster's electronic structure at the frontier orbitals. Compound **13,** may be thought of as two As_7 clusters that are bound by a Hg-As dimer. Figure 22 shows the density of states of the As_7^{3-} cluster, the $[Zn(As_7)_2]^{4-}$ motif, and the $[HgAs(As_7)_2]^{3-}$ cluster. The total and projected density of states are given, where the density of states are projected from the cluster orbitals of As_7^{3-} using a fragment analysis. The blue line is the projected density of states of the three closely spaced levels at the Fermi energy of As_7^{3-}, which are indicated in Figure 22 and are labeled Shell 3. The next two deeper sets of closely spaced states are labeled Shell 2 and Shell 1, and the lowest set of unfilled orbitals of As_7^{3-} is labeled as Shell 4. Note that the use of the term "shell" does *not* imply that these are degenerate states in a nearly-free electron model, but rather a grouping of molecular orbitals with similar energies. The density of states plotted negatively are projected from the Hg-As linker in which σ states of the molecule are indicated with a maroon line, and the π states are indicated with a magenta line. The alignment of σ and π states with projected cluster states outside of the expected shell regime indicates splitting of the levels due to covalent interactions. The projected density of states shows that the cluster building blocks still retain much of their initial shell structure, but there is significant splitting in the states due to mixing between the As_7 cluster and the Hg-As linker. This mixing is rather complicated, and for comparison we have plotted similar projected density of states in Figure 20b. The -3 charge state of the complex is due to the formation of two bonding and antibonding pairs, which

reduce the oxidation state by 4 e^-, and the additional As atom, which has an odd number of valence electrons. The increase in mixing results in a decrease in the band gap energy of the cluster solid which is seen from the mixing of states that drop below the LUMO state of the As_7^{3-}. This is also seen in the DOS of the solid calculated using the experimentally determined X-ray structure in the VASP code. The DOS shown in Figure 20b shows the splitting of the lowest unoccupied state as discussed above and further confirms that the lowest state has significant contributions from As_7 and the linker Hg/As sites.

We have found that the same specific cluster states interact with the linkers, even when different linkers are used. The measured band gap is found to decrease with increasing complexity of the covalent linker; the band gap is largest for materials in which the clusters are joined by Zn and Cd atoms, while the Hg-Hg dimer based material has a lower band gap, and the Hg-As linked clusters have an even lower band gap. This is caused by the covalent splitting of the cluster's molecular orbitals, which broadens the shells near the band gap reducing the band gap energy.

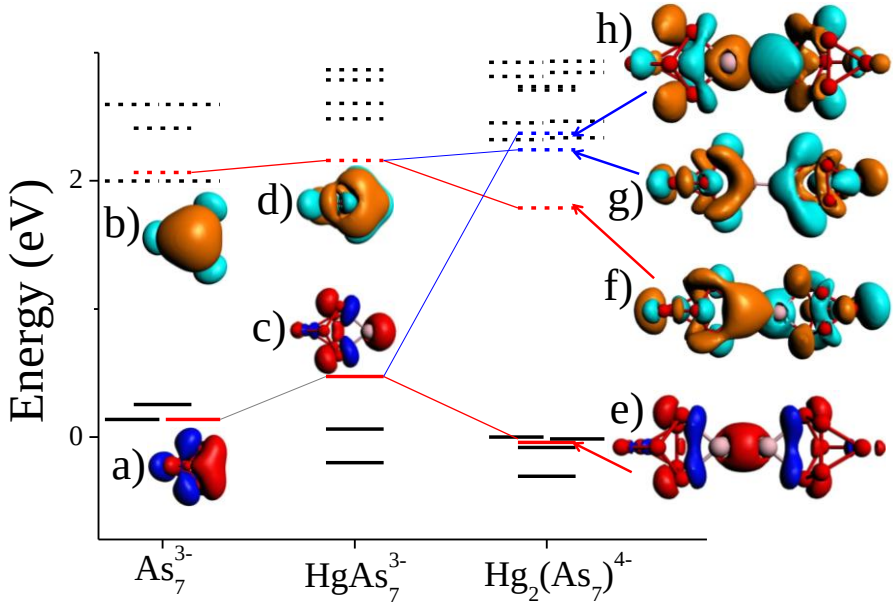

***Figure 21**. Molecular orbital diagram for As_7^{3-}, $HgAs_7^{3-}$, and $[Hg_2(As_7)_2]^{4-}$. A) and B) are the HOMO-1 and LUMO+2 of As_7^{3-}, c) and d) are the HOMO and LUMO of $HgAs_7^{3-}$ and E), F), G), and H) are the HOMO-2, LUMO, LUMO+1 and LUMO+4 of $[Hg_2(As_7)_2]^{4-}$.*

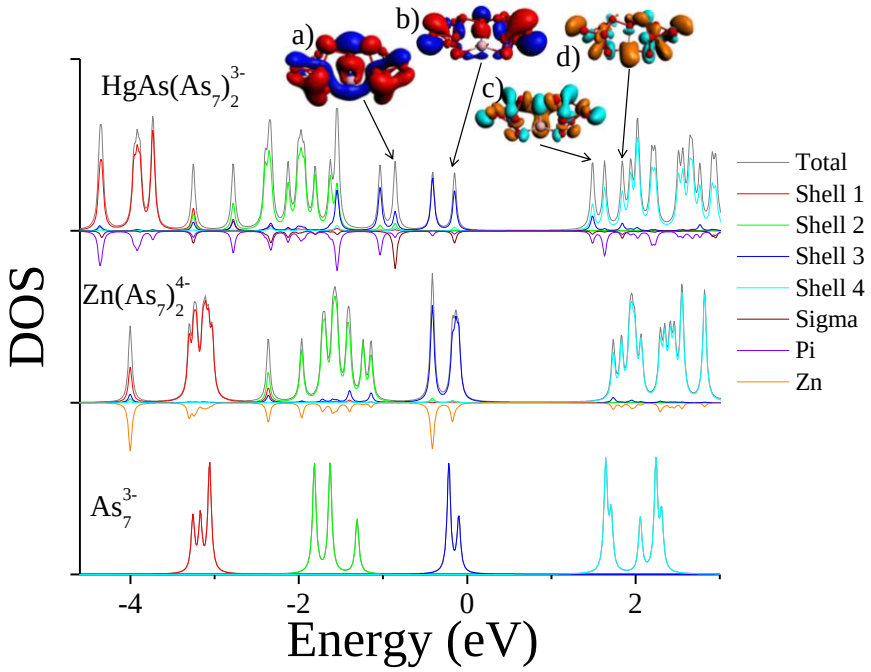

Figure 22. Density of states for $[HgAs(As_7)_2]^{3-}$, $[Zn(As_7)_2]^{4-}$, and for As_7^{3-}. Shells 1-4 are the projected density of states for the cluster molecular orbitals which are closely grouped on As_7^{3-}. The negative states are projected from the HgAs molecule, which links the clusters; Σ indicates sigma states of the HgAs molecule, and Π indicates pi states of the molecule

Effect of internal electric field for three-dimensional structures

Compounds $[K\text{-crypt}]_2[Zn(As_7)_2Cs_2]$ 2*en* , **14**, and $[K\text{-crypt}]_2[Cd(As_7)_2Rb_2]$ 2*en*, **15**, are constructed from the same kinds of cluster building block as $[K\text{-Crypt}]_4[Zn(As_7)_2]\cdot 2en$, **10** and, and $[K\text{-Crypt}]_4[Cd(As_7)_2]\cdot en$, **11**, however they are linked differently through Cs, and Rb into unusual linked-layer (three-dimensional) structures and have the largest band gap energy of the clusters studied here, 2.16 eV and 2.21 eV. This corresponds to an increase in band gap energy of 0.17 eV for Zn linked clusters and 0.34 eV for the Cd linked clusters. Previous studies on the effect of architecture on the band gap energy of ionic cluster assemblies have found that internal electric fields may increase the band gap energy of cluster assemblies that are linked by naked alkali cations. To test this hypothesis, we have calculated the HOMO-LUMO gap of the $[Zn(As_7)_2]^{4-}$ and $[Cd(As_7)_2]^{4-}$ clusters as a function of point charges that are located in the position of the cations. Figure 23 shows that at zero field Zn has a slightly larger gap energy of 0.03 eV, and that both have increasing gap energies with increasing internal electric field. The maximum gap is found with point charges of +0.5 e^-, and that the two curves cross at +0.7 e^-. As the Bader charges on the ions correspond to around +0.7, we believe this charge corresponds to the best estimate of the internal electric field. At this field strength, the Zn linked cluster has increased its gap energy by 0.20 eV, and the Cd linked has increased by 0.23 eV which agrees reasonably well with increase in band gap energy observed in **14** and **15**. This shows that the increase in band gap energy of **14** and **15** is caused by the internal electric field generated by the alkali counterions which link the covalently linked cluster species.

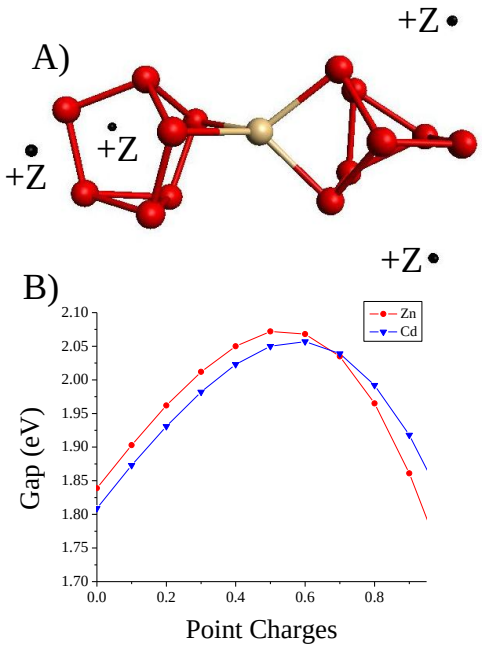

Figure 23. A) Geometry of $[Cd(As_7)_2]^{4-}$ model with point charges in the position of Cs. B) HOMO-LUMO gap as a function of point charge Z for $[Cd(As_7)_2]^{4-}$ and $[Zn(As_7)_2]^{4-}$.

Band Gap Energy Tuning: Role of Electronegativity

We have synthesized a series of covalently linked cluster with different electronegativity. Among these we have compared two structures (Au and Zn linked, compounds **5** and **10**) with fairly different electronegativity. Based on Pauling's scale electronegativity of Au and Zn are 2.54 and 1.65, respectively. The structure of [K-Crypt]$_4$[Zn(As$_7$)$_2$], **10**, was similar to that of [K-Crypt]$_4$[Au$_2$(As$_7$)$_2$], **5**, except that Au$_2$ is replaced by a single Zn atom. While the structure is similar, the substitution of Au$_2$ by Zn increases the band gap from 1.69 to 1.99 eV. To probe the origins of this increase, representative electronic structure, studies on K$_4$(As$_7$)$_2$Zn were carried out and the results compared with those for K$_4$(As$_7$)$_2$Au$_2$ clusters. A Hirshfeld charge analysis indicated that while the net charge on each Au atom is -0.02, the charge on the Zn sites is +0.17, showing greater charge transfer to the arsenic motif in the Zn assembly. As the enhanced charge transfer lowers the HOMO states on the arsenic anion, a decrease in the electronegativity of the linker results in an increase in the band gap of the solid.

Band Gap Energy Tuning: Role of dimer

We have synthesized different types of covalently linked clusters where linkers are dimeric in nature. These are [K-Crypt]$_4$[Au$_2$(As$_7$)$_2$], **5**; [K-Crypt]$_4$[Hg$_2$(As$_7$)$_2$], **12**; and [K-Crypt]$_4$[Pd$_2$(As$_7$)$_2$], **16**, respectively (Figures **3a, 5c** and **10a**). The band gap energy of Pd linked clusters is lower than the other dimeric linked clusters. To understand why the band gap energy of the $[Pd_2As_{14}]^{4-}$ motif is smaller than that of nearly all previously studied As-based cluster assemblies, we examine the molecular orbital diagram of the As_7^{3-} and Cs$_4$[Pd$_2$As$_{14}$] clusters in Figure 24b. The intrinsic band gap energy of As_7^{3-} is 1.80 eV so we have aligned the two nearly degenerate lone pair orbitals from $[Pd_2As_{14}]^{4-}$ with the HOMO of As_7^{3-}. The lone pair orbitals in As_7^{3-} and Cs$_4$[Pd$_2$As$_{14}$] are found on the equatorial atoms and have similar character as shown in Figure 24b. The Pd$_2$ Σ_u orbital lies 0.36 eV higher than these lone pair orbitals. The molecular

orbital of the HOMO is constructed from the $4d_z^2$ orbitals of the Pd dimer and is localized almost exclusively on the Pd. The LUMO as shown in Figure 10b is an orbital which mixes with both As_7 motifs through the Pd atoms resulting in a new and slightly lower LUMO than As_7^{3-}, and the LUMO+1 has significant charge density on the Pd atom. The result is that we can think of the Pd dimer as creating a set of states that are embedded in the band gap of the As_7^{3-} cluster, which decrease the band gap energy.

(a)

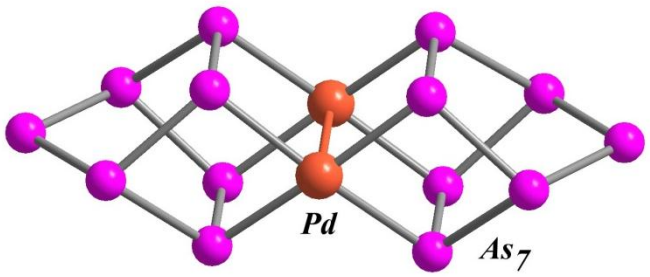

(b)

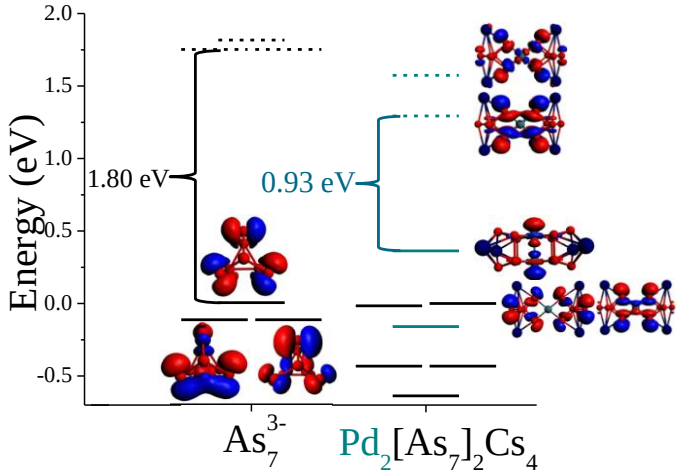

Figure 24. (a) The cluster unit of **16**, $[K\text{-crypt}]_4[Pd_2(As_7)_2]3en$. [K-crypt] and ethylendiamine molecules are not shown for clarity. (b) Molecular orbital diagram from $[As_7]^{3-}$ and $Pd_2(As_7)_2Cs_4$. The HOMO−2, HOMO−1, and HOMO for $[As_7]^{3-}$ are plotted, along with the HOMO−2, HOMO−1, HOMO, LUMO, and LUMO+1.

Band Gap Energy Tuning: Role of Charger Transfer Complex

All the above mentioned clusters are either zero-dimensional or two-dimensional or three-dimensional in nature. To know the role of one-dimension we have synthesized clusters with a metal carbonyl (charge transfer complex) which can be linked to form the one-dimensional structures. Charge-transfer complexes are well known as strong absorbers of visible light, so the incorporation of such complexes within a cluster-assembled material may affect the optical properties of the material. We examine the effects on the band gap energy of cluster assemblies from an As_7^{3-} bound to one or two $M(CO)_3$ molecules, in which M is the group VIb elements, Cr, Mo, and W. We examined zero-dimensional (0D) assemblies of $[As_7Cr(CO)_3]^{3-}$, **18**; 1D assemblies of $[As_7Cr(CO)_3]^{3-}$ linked by Cs atoms, **21**; 0D assemblies of $[(en)Mo(CO)_3As_7(Mo(CO)_3)_2]^{3-}$, **19**, and $[(en)W(CO)_3As_7(W(CO)_3)_2]^{3-}$, **22**, and 1D assemblies

of $[As_7Mo(CO)_3]^{3-}$, **20**, and $[As_7W(CO)_3]^{3-}$, **23**, linked by Cs atoms (Figure 11). To understand the effects of charge-transfer ligands on the band gap energy, we have done theoretical investigations to understand the origins of the variations in the band gap energy. The small variation in the band gap energies of the $[As_7M(CO)_3]^{3-}$ cluster assemblies is due to the small perturbation of the electronic structure of the cluster and the close alignment of the metal carbonyl orbitals and lone pair orbitals of the arsenic cluster. The band gap energy of the isolated $[As_7]^{3-}$ cluster is 1.80 eV, and the variations of the 1D $[As_7M(CO)_3]^{3-}$ clusters and isolated $[As_7Cr(CO)_3]^{3-}$ cluster are all within 0.10 eV of that band gap energy. Because bonding between the cluster and metal-carbonyl is due to charge transfer, the change in the electronic structure from the pure cluster to the complex does not involve significant reordering of the electronic levels typical of covalent bonds. Furthermore, the lone pair HOMO of the cluster is closely aligned in energy with the HOMO of the metal carbonyl complex so the "valence band edge" of the cluster is unaffected. The LUMO of the metal carbonyl is also quite high in energy, so it does not affect the "conduction band". The end result is that the effect on the band gap energy by the single metal complex is quite small, at least when the complexes are similar.

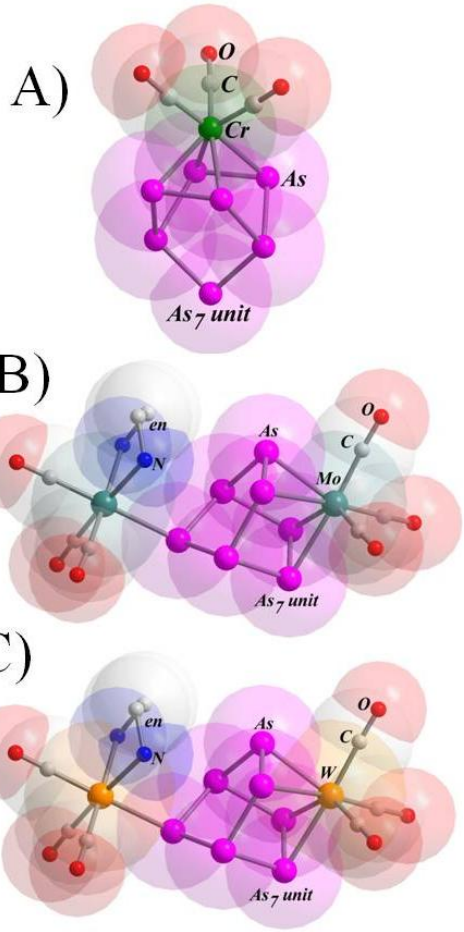

D)

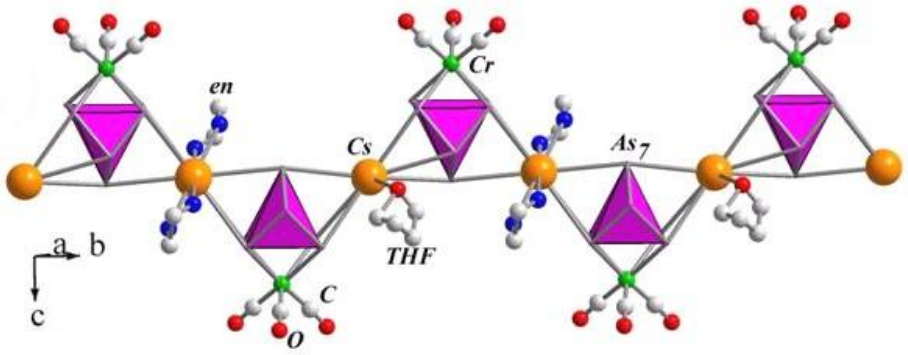

Figure 25. X-ray crystallographic structures of: A) zero-dimensional cluster $[K\text{-crypt}]_3[As_7Cr(CO)_3]$, **18**; B) zero-dimensional cluster $[K\text{-crypt}]_3[(en)Mo(CO)_3As_7Mo(CO)_3]$, **19**; C) zero-dimensional cluster $[K\text{-crypt}]_3[(en)W(CO)_3WAs_7(CO)_3]$, **20**; D) One-dimensional chain structure in A) $[K\text{-crypt}]_2[As_7Cr(CO)_3Cs]$.en.THF, **21**. K-crypt has not shown for clarity.

Isolation of new electron deficient As_7^{2-} cluster

During the course of this linked clusters study we have synthesized an electron deficient cluster $[K(2,2,2\text{-crypt})]_2[As_7]\cdot THF$, **24**, whose structure, magnetic behavior, electron paramagnetic resonance (EPR) spectrum, electrochemistry, solid-state band gap and UV-Vis spectrum are presented here.

Crystals of **24** in high yield were made by precipitation of a solution of a precursor K_3As_7 in ethylenediamine and excess of crypt. Single-crystal X-ray structure determination showed the presence of one asymmetrical As_7 motif, two [K(2,2,2-crypt)] units and one THF molecule (Figure 26a). The presence of two $[K(2,2,2\text{-crypt})]^+$ ions per cluster indicates that the cluster is a dianion. According to the simple electron-transfer model of Zintl and Klemm, $[K(2,2,2\text{-crypt})]_2[As_7]$.THF, **24** contains 37-valence electrons, so compound, **24** is a radical anion. It is the first seven-atom 37-electron system of group 15. The As – As bond distances in **24** are in the range of 2.1673 – 2.7397 Å (av. 2.4272 Å) and the clusters are arranged in *ABAB*…. fashion in the *ab* plane (Figure 26b).

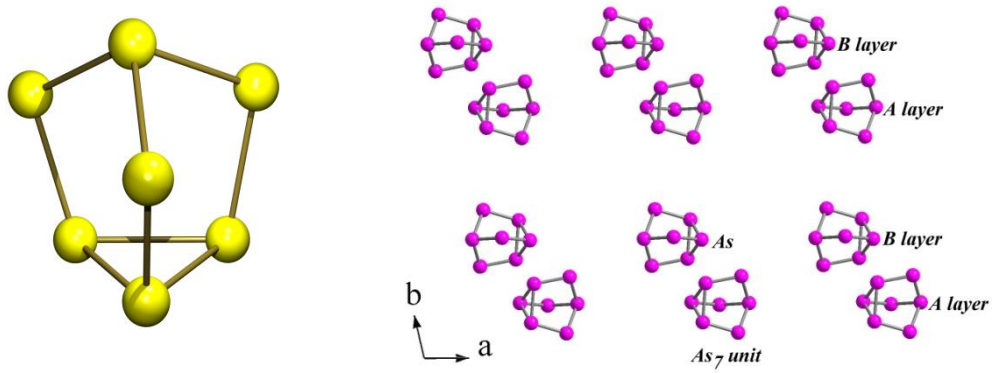

(a) (b)

Figure 26 (a) The asymmetric unit As_7^{2-} (b) ABAB arrangement of the As_7^{2-} cluster units in ab plane.

The presence of an unpaired electron localized on individual cluster units leads to interesting behaviors. We investigated the magnetic properties, EPR spectrum, electrochemistry and solid-state band gap of compound, **24**. Magnetic studies were carried out on powder samples using a SQUID magnetometer over the temperature range 1.8 K to 160 K at a magnetic field of 100 Oe. The temperature dependence of the magnetic susceptibility (χ_M) is shown in Figure 27a, showing the paramagnetic behavior. The Curie-Weiss fit from T = 1.8 K to 70 K shows a small value of Curie-Weiss temperature θ_W = - 0.5 ± 0.3 K, indicating that there is minimal intermolecular interaction. The derived effective magnetic moment (μ_{eff}) at 160 K is 1.62 ± 0.07 μ_B. The EPR spectra were recorded on powder samples at 100 K (Figure 27b) and the spectra appear to be isotropic with g = 2.003, which shows good agreement with the calculated g factor of 1.996 for an isolated $[As_7]^{2-}$. These magnetic and EPR data confirm that the cluster has an unpaired electron, which is in good agreement with the single-crystal structure. Compound **24** and K_3As_7 are soluble in DMF, and this solubility has enabled us to electrochemically study the redox chemistry. Cyclic voltammetry measurements were carried out on 1 mM DMF solutions of

As_7^{3-} (Figure 28a). The voltammogram shows a reversible single-electron oxidation/reduction process corresponding to the As_7^{3-}/As_7^{2-} redox pair. Control experiments with only solvent/electrolyte did not show any redox active impurities in the solvent or the electrolyte. The reduction/oxidation potentials of As_7^{2-}/As_7^{3-} are -0.5 V and -0.15 V vs. the Ag^+/Ag reference electrode. We have also measured the solid-state band gap of **24** in powder form using diffuse reflectance spectroscopy, and the Kubelka-Munk model. Using the equation, the band gap of compound, **24** was obtained by extrapolating to the x-axis with the linear fit to a plot of $(\kappa h\nu)^{1/n}$ *vs.* $h\nu$ and the estimated value of band gap is (E_{bg}) = 1.41±0.03 eV (Figure 28b).

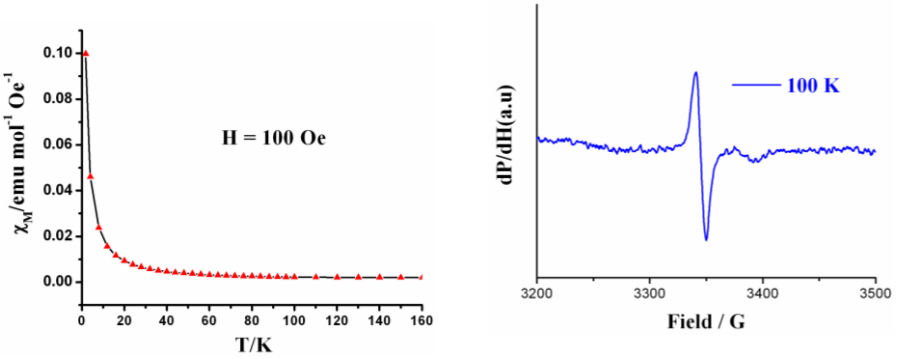

(a) (b)

Figure 27 (a) χ_M vs. T data of **1** at 100 Oe and (b) EPR data of **24** at 100 K.

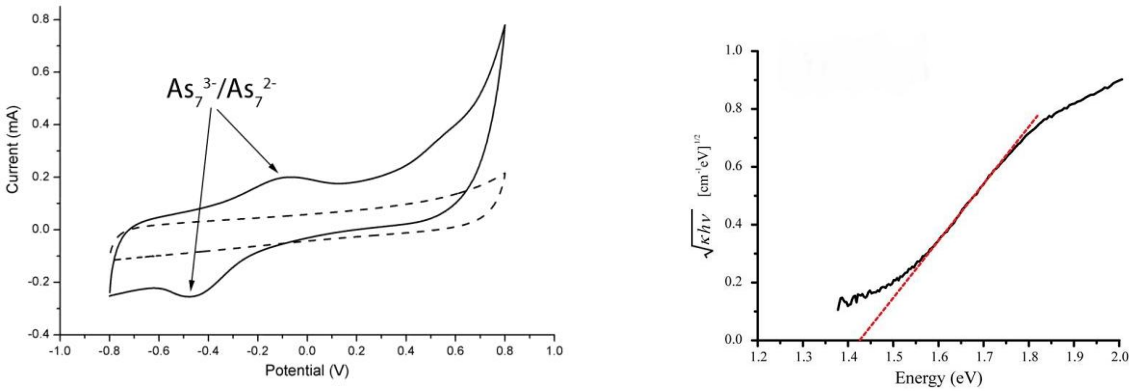

(a) (b)

Figure 28 (a) Cyclic voltammogram of 1 mM solution of As_7^{3-} in DMF, scanned from -0.8 V to 0.8 V at the scan rate of 100 mV/s. Dashed line represents the blank experiment with DMF and 0.1 M $LiBF_4$. (b) Tauc plot showing the band gap determined from the optical absorption spectra of compound $[K(2,2,2\text{-crypt})]_2[As_7].THF$, **24**.

The difference in electronic structure between the electron deficient compound, **24** and $[As_7]^{3-}$ is revealed in the UV-Vis spectra. The crystal structure of $[K\text{-crypt}]_3[As_7]$ has not been reported. We have synthesized K_3As_7 in solution and compared the UV-Vis spectrum of this compound with that of compound, **24** in a dimethylformamide solution (Figure 29a). The experimental spectrum compared well with the calculated UV-Vis spectra of $[As_7]^{2-}$ and $[As_7]^{3-}$ as shown in Figure 29b, and Figure 29c. We have also calculated the optical absorption

spectrum of a singly charged As_7 cluster, $[As_7]^-$ and it shows no significant absorbance peaks until 3.05 eV, which demonstrates that $[As_7]^{2-}$ is the origin of the 2.2 eV absorption.

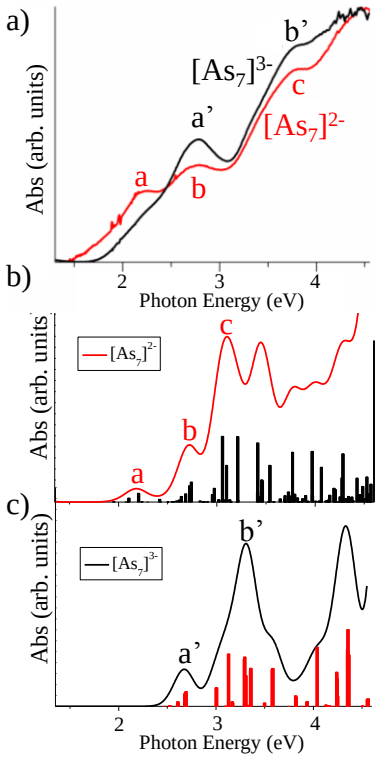

Figure 29 a) Experimental UV-Vis spectra of synthesized K_3As_7 ($[As_7]^{3-}$) and compound $[K(2,2,2\text{-crypt})]_2[As_7]$.THF, (**24**) ($[As_7]^{2-}$) in dimethylformamide. Simulated UV-Vis spectra for b) $[As_7]^{2-}$, and c) $[As_7]^{3-}$ in dimethylformamide.

First principles theoretical studies within a gradient corrected density functional framework were undertaken to provide further insight into the observed features. Two kinds of studies were undertaken. In one, calculations on representative free clusters were carried out using the deMon2k code to understand the nature of bonding and the associated structural changes. The calculations on the solid used a periodic supercell with the Vienna Ab-initio Simulation Package (VASP) and focused on the electronic structure of the crystal and the absorption spectra.

Previous theoretical studies have established that the ground state of an K_3As_7 cluster (composed of $[As_7]^{3-}$ motifs) is a C_{3v} structure (see Figure 30). The electronic structure of the cluster is marked by three degenerate states occupied by three spin-up and three spin-down electrons (see Figure 30c-f). The removal of a K atom to form K_2As_7 (leading to $[As_7]^{2-}$ species) results in an unfilled HOMO leading to a Jahn-Teller distortion that can be best described as a contraction of the distances between atoms in the equatorial triangle (see Figure 30b). The $[As_7]^{2-}$ cluster may undergo a pseudorotation in which the contracted As pair (bottom two atoms in Figure 16b) moves to an adjacent pair, with an energy barrier of only 0.05 eV, which likely contributes to the observed disorder in the crystal structure. The distortion reduces the symmetry from that of the $[As_7]^{3-}$ motif leading to a distribution of the As - As distances as observed in the experiment. Even more interesting are the new electronic orbitals (Figure 30g, h, and i) that show that the spin density of the unpaired electron is largely localized (see blue region) in the covalent bonds between the atoms in the basal triangle and those in the upper triangle (see Figure 30b). Further, the uneven spin occupation leads to a relative shifting of the spin up and down orbitals. Its impact is more clearly seen in the band structure of the solid obtained using the

VASP code with a periodic cell containing two As_7 and four cryptated K atoms. Figure 31a shows the one-electron levels in the solid and a pair of unfilled levels in the minority band (as there are two As_7 units in a periodic cell). We also calculated the absorption spectra using a time-dependent density functional approximation; the results are shown in Figure 31b.

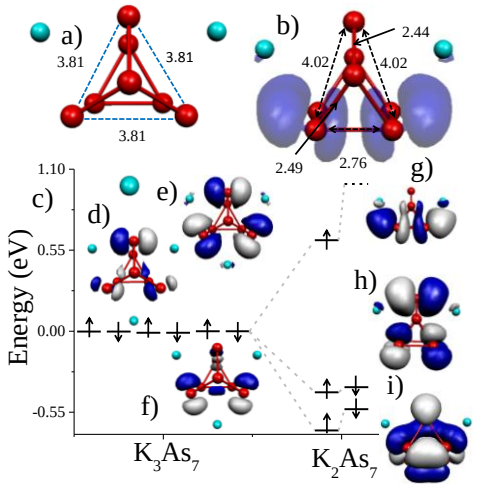

Figure 30. Calculated structure of a) K_3As_7 and b) K_2As_7 with spin density. c) shows the energies and wave functions of the one electron levels of K_3As_7 (d - f) and K_2As_7 (g - i).

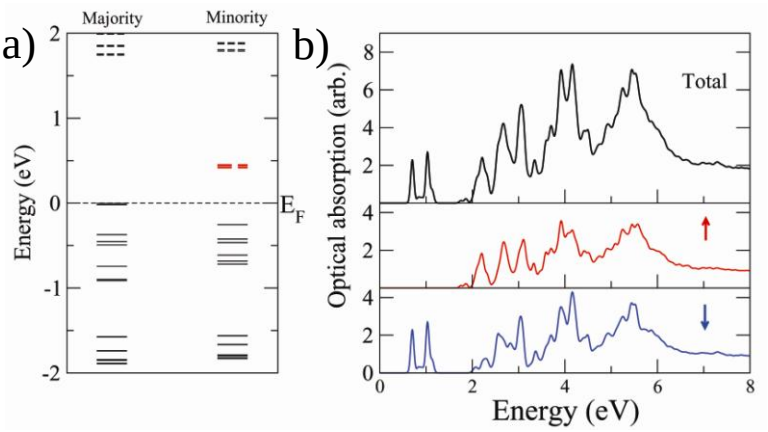

Figure 31. a) Calculated one-electron levels at the Gamma point of the $[K\text{-crypt}]_2[As_7]$ material and b) the calculated absorption spectra.

The spin-up channel leads to a band gap of around 1.7 eV while the minority states have a band-edge starting at 0.6 eV. Due to limitations in our experimental techniques, we are unable to observe band gaps below 1.0 eV. Consequently, the observed band-gap at 1.41 eV (Figure 28b) corresponds to the majority spectrum that has a gap of around 1.7 eV (Figure 31a). An analysis of the geometry and the electronic states confirms the picture from the cluster calculations that the resulting solid has disordered structure with spin moments localized on individual motifs. A comparison of the energy for forced ferromagnetic and anti-ferromagnetic configurations (Figure 32) shows a difference of only 11 meV per cluster. The small coupling is consistent with the solid behaving like a paramagnet.

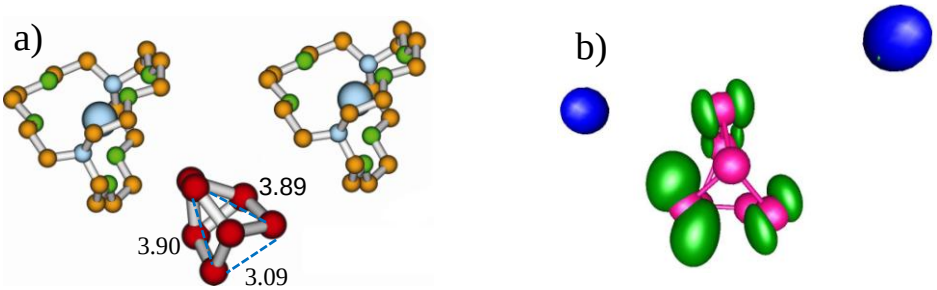

Figure 32. a) Calculated geometries and b) electron spin density (in green) of the $[K\text{-crypt}]_2[As_7]$ in a ferromagnetic (FM) solid state. Bond lengths are in angstroms (Å).

Cluster Characterization and Ionization

Mass spectrometry plays a major role in many of the techniques employed to characterize the structural, dynamical, and electronic properties of superatom building blocks of tailored materials. A phenomenon we exploit in clusters is an enhancement in ionization under ultrafast laser pulses. This enhancement results in the lowering of the laser intensity required to observe ion signal from higher atomic charge states resulting from Coulomb explosion of clusters. Here, we explore the effect of using an early-group transition metal as an electron source in the formation of small silicon and germanium clusters on the observed enhancement in ionization. Intensity selective scanning is used to measure the onset of ion signal for the atomic charge states of silicon, germanium, zirconium, and oxygen. In the studies kinetic energy release (KER) values resulting from Coulomb explosion of silicon clusters with zirconium were measured and compared to those of pure silicon clusters previously observed using a copper electron source. A significant increase in ionization enhancement is observed upon addition of zirconium metal. Germanium shows a larger enhancement in ion signal than does silicon, indicating that atomic mass may be significant. Pure zirconium oxide clusters also were investigated for comparison and ionization trends were explored.

During the course of the investigations, the electronic properties of select transition metal silicide diatomics were also studied with the aid of anion photoelectron imaging spectroscopy and theoretical methods. The transition metal silicide diatomic anions, which are produced in a laser vaporization source and mass selected using a time-of-flight (TOF) mass spectrometer, were photodetached using laser pulses of 532 nm (2.33 eV), revealing the unique photoelectron angular distributions and electron binding energies. Density functional theory (DFT) and *ab-initio* unrestricted coupled cluster singles and doubles (triplets) *UCCSD(T)) methods were utilized to assign the ground and excited electronic states of the neutral and anionic diatomics.

During subsequent studies, a combined experimental and theoretical investigation was undertaken of small ZnO-based clusters. A laser vaporization source and a time-of-flight (TOF) mass spectrometer was used to produce and identify anionic clusters in the Zn_nO_m (n = 1-6, m = 1-7) size regime. The adiabatic detachment energy (ADE) and vertical detachment energy (VDE) of $Zn_3O_3^-$ and $Zn_3O_4^-$ clusters were determined by anion photoelectron spectroscopy. We have utilized density functional theory (DFT) calculations to explore the possible geometries of neutral and anionic Zn_3O_m (m = 3,4,5) clusters, while the theoretical ADE and VDE values are compared with experimental results. The experimentally observed relative abundances between the $Zn_3O_m^-$ (m = 3,4,5) clusters were investigated through calculations of the detachment

energies, dissociation energies and HOMO-LUMO gaps. We find that the Zn_3O_3 cluster maintain enhanced stability compared to their oxygen-rich counterparts.